Influence of PEG-containing cation on molecular state of water in water – Acetate based ionic liquids mixtures

D. Kurchavov, U. Rustambek, M. Haddad, A. Ottochian, G. Lefèvre, I. Ciofini, V. Lair, P. Volovitch

Journal of Molecular Liquids 367 (2022) 120564

Contents lists available at ScienceDirect

Journal of Molecular Liquids

journal homepage: www.elsevier.com/locate/molliq

Influence of PEG-containing cation on molecular state of water in water – Acetate based ionic liquids mixtures

D. Kurchavov [a], U. Rustambek [a], M. Haddad [b], A. Ottochian [c], G. Lefèvre [a], I. Ciofini [c], V. Lair [a], P. Volovitch [a,*]

[a] Chimie ParisTech, PSL University, CNRS, Institut de Recherche de Chimie Paris (IRCP), F-75005 Paris, France
[b] PSL University, Chimie ParisTech, CNRS UMR 8060, Institute of Chemistry for Life and Health Sciences, CSB2D Team, 75005 Paris, France
[c] PSL University, Chimie ParisTech, CNRS UMR 8060, Institute of Chemistry for Life and Health Sciences, TCM Team, 75005 Paris, France

ARTICLE INFO

Article history:
Received 17 April 2022
Revised 11 September 2022
Accepted 6 October 2022
Available online 12 October 2022

ABSTRACT

Two acetate ionic liquids (ILs) based on *N*-methyl-pyrrolidinium cation with etheric ($mPEG_n$-) and aliphatic (butyl-) substitutions were synthetized. Electrochemical potential windows (EPWs) were measured on a glassy carbon electrode. The results revealed that introduction of etheric group in the IL structure constricts the EPW if compared with aliphatic substitution. The binary mixtures of ILs with water were characterized by Raman, Attenuated Total Reflectance Fourier Transform Infrared (ATR-FTIR) spectroscopies and Molecular Dynamics (MD) simulations. Intermolecular hydrogen bonds between acetate anions and ether-substituted cations have been found. Detailed analysis of local structure of water in these mixtures by ATR-FTIR and MD simulations indicates that "free water phase" clusters appear when the molar ratio between water and IL, $n(H_2O)/n(IL)$, is larger than 3 in case of [BMPyr]AcO and larger than 7 for [$mPEG_n$MPyr]AcO. The evolution of the specific conductivity of water-ILs mixtures with water content well correlates with the modification of the water state.

1. Introduction

Room temperature ionic liquids (RTILs or ILs) are compounds which entirely consist of ions and exist in liquid state at the temperatures below 100 °C. They attract enormous interest because of a wide range of possible applications, from organic synthesis and catalysis to analytical chemistry and electrochemical applications thanks to a high solubility of a wide range of inorganic, organic and polymeric materials in them [1–3]. RTILs are widely employed as electrolytes for electrochemical applications [4,5] because of their enhanced electrochemical and thermal stability [6–8], their relatively high conductivity [9], low volatility [10] and non-flammability [11]. The disadvantages of RTILs as electrolytes are their relatively high viscosity and the relatively narrow temperature interval in which they stay in the liquid state [12].

Physico-chemical properties, such as specific conductivity and viscosity of RTIL, can be adjusted by varying the nature of the cations and anions [7,13–16]. Such a solution is however unsuitable for task-specific RTILs which should contain specific functional groups. In this case, the improvement of viscosity and specific conductivity can be achieved by a small dilution with conventional organic solvents [17–19]. Nevertheless, considering RTILs applications as "green" solvents, their dilution by toxic organic solvents is undesirable [20] and water looks more attractive, especially, for the applications in water-based systems and biochemistry [21,22].

Viscosity decrease [23–25] and conductivity increase [25,26] upon dilution by water can however be accompanied by the narrowing of the electrochemical potential window (EPW) because of water decomposition [25,26]. The latter effect can be reduced if water electrochemical reactivity is controlled either by limiting water content or by strong water – IL interactions, e.g. intermolecular hydrogen bonding [27,28]. Understanding these interactions is therefore important for numerous applications.

In the literature two types of ILs are distinguished accordingly their miscibility with water: (1) hydrophobic ILs which pick up minimum of water and saturate at low water concentration, and (2) hydrophilic ILs which are infinitely miscible with water [29]. Molecular Dynamic (MD) simulations demonstrated that the hydrophilicity is controlled by the nature of ions. For instance, long aliphatic tails in cations increase hydrophobicity because of the formation of nonpolar domains [30]) but also by their interactions with water and between them [31–34]. A relative strength of the interactions between water and IL ions compared with the interactions between the anions and cations of the IL plays a crucial role in defining the observed hydrophilicity [30,31,35,36]. For instance, both simulation [37] and experimental observations by infrared spectroscopy [38,39] demonstrated in the water mixtures with the ILs containing hydrophobic anions water molecules form

* Corresponding author.
E-mail address: polina.volovitch@chimieparistech.psl.eu (P. Volovitch).

https://doi.org/10.1016/j.molliq.2022.120564
0167-7322/

self-associated hydrogen (H) - bonded water phase inclusions. Structural nanoheterogeneity in water-rich regions lead to the formation of so-called "water-pockets" at low and continuous water-cluster at high water concentrations [40].

Water clusters formation can be prevented in RTILs containing hydrophilic anions, such as NO_3^- and BF_4^- [37] or acetate ion CH_3-COO^- (further named as AcO^-) [41]. In these cases MD simulations revealed that the H-bonds lead to bridged Anion···HOH···Anion structures, preventing water to water self-association. Water-anion hydrogen bonds can be even stronger than cation–anion interactions [25,39,42,43], in particular very strong H-bonding was reported for the $CF_3CO_2^-$ anion due to its high basicity [39]. In associates with IL water molecules can act as a double donor (DD), with a ratio of one water molecule for two of IL ion pairs (1 H_2O: 2 IL), or as a single donor (SD), with one water molecule per one IL ion pair (1 H_2O: 1 IL) [44,45].

Less is known about the interaction of water with IL cations. Recently, some evidences of hydrogen bonds formation between water and hydrophilic 1-butyl-1-methyl-pyrrolidinium cation were reported [46]. Interactions between water and ions of RTIL can also affect the properties of RTIL as a solvent, for instance modifying molecular structures of nucleobases in the solution for biological applications [47] and affecting the solvation free energy [48].

To sum up, although the effect of RTIL anions on the water state in water-RTIL mixtures was a subject of thorough investigations, water-RTIL cations interactions have not yet been intensively studied. The reason for this is that water-RTIL cation interactions are expected to be significantly weaker than H-bonding of water with RTIL anions. The situation can be however different in the presence of hydrophilic substituent groups, such as, ether groups, in the chains of the cations. To the best of our knowledge, no systematic study of the effect of the hydrophilic groups in the cation on the water - RTIL interactions has been published. Inserting hydrophilic groups into the structure of cations of ILs can be however very interesting because it can improve their water absorption capacity. Design of new water-miscible RTILs can hence be improved by intelligent modification of the substituted chains in the IL cation. Poly-ether groups containing compounds are promising candidates expected to form intermolecular hydrogen bonds with water [49]. Polyethylene glycols (PEG) are considered as biodegradable, biocompatible compounds and are widely used in cosmetics, pharmaceutical industry and in nanochemistry [50–52]. For electrochemical applications poly-ether chains can be interesting because they improve transport properties of ILs [53] and they can lead to the complexation of metal cations, such as Li^+ [53,54], Mg^{2+} [55–57] and Na^+ [58]. Understanding interactions of PEG-substituted RTIL cations with water in water–RTIL mixtures and mastering the effect of water content on these interactions and resulting properties are hence of high interest for a rational design of new water-miscible RTILs.

Thus, the main objective of this work is to explore from both experimental and theoretical points of view the molecular state of water in H_2O-IL mixtures of PEG-substituted cation in *N*-methyl-pyrrolidinium (MPyr) acetate (AcO) ILs. This is here achieved via several intermediate goals:

a) **synthesis** of two acetic ionic liquids with hydrophilic poly-ether.

(-O-CH_2-CH_2-)$_n$)) substituted cation ([mPEG$_n$Pyr]AcO, further named as etheric IL or IL**E**), and hydrophobic aliphatically (butyl (-C_4H_9)) substituted cation ([BMPyr]AcO, further named as aliphatic IL or IL**A**);

b) **characterization** of their electrochemical properties: specific conductivity and electrochemical potential window;

c) **analysis of the effect of water content** on the molecular state of water in water-RTIL binary mixtures in a wide composition range (from several % to more than 90 % of water) using vibrational spectroscopies;

d) **rationalization** of the effect of PEG$_n$-substitution in the cation on the molecular state of water in the mixtures by MD simulations of pure ionic liquids and their mixtures with water.

2. Experimental

2.1. Synthesis of RTILs

2.1.1. Materials for synthesis

The following commercially available compounds were used for synthesis: Methoxy-terminated poly(ethylene glycol) (mPEG$_7$, CAS no. 9004-74-4, M.W. 350), 4-toluenesulfonyl chloride (TsCl, CAS no. 98-59-9, 99 %), 4-dimethylaminopyridine (DMAP, CAS no. 1122-583, 99 %), triethylamine (CAS no. 121-44-8, 99.5 %), anhydrous potassium iodide (KI, CAS no. 7681-11-0, 99 %), *N*-methylpyrrolidine (CAS no. 120-94-5, 97 %), silver nitrate ($AgNO_3$ CAS no. 7761-88-8, ≥99 %), ethyl acetate (CAS no. 141-78-6, ≥99.5), toluene (CAS no. 108-88-3, 99.8 %), 1-butyl-1-methyl-pyrrolidinium iodide (CAS no. 56511-17-2) supplied by Sigma-Aldrich. Acetone (CAS no. 67-64-1), chloroform (CAS no. 67-66-3), methanol (CAS no. 67-56-1), cyclohexane (CAS no. 110-82-7), acetic acid (CAS no. 64-19-7, ≥99.7 %), ion exchange resin Amberlyst® A-26 (OH) (CAS no. 39339-85-0) supplied by VWR. All chemicals were used as received.

2.1.2. Synthesis procedure

Synthesis of IL**A**. Synthesis of 1-Butyl-1-methyl-pyrrolidinium acetate (IL**A**) is presented on Scheme 1.

Aqueous solution of 1-butyl-1-methylpyrrolidinium iodide (6 g, 0.022 mol) was passed dropwise through a chromatography column packed with Amberlyst A-26 hydroxide form (40 g). One equivalent amount of acetic acid was added to the resulting solution. Neutral pH was controlled with a pH meter. The water was removed by evaporation under vacuum using rotary evaporator at 60 °C. The absence of iodide in the prepared IL was verified by the reaction with the excess of 0.1 M $AgNO_3$ aqueous solution. No precipitates indicated that the I^- content in IL was inferior to the value given by the solubility product of AgI (K_{sp}(AgI) = 1.$5{\cdot}10^{-15}$).

The product composition was confirmed by ^{1}H, ^{13}C-Nuclear Magnetic Resonance (NMR) and high resolution mass spectrometry HRMS. For the IL**A,** [BMPyr]AcO, the positive mass over charge ratios *m*/*z* detected in atmospheric pressure chemical ionization (APCI-Orbitrap) (+) were: *m*/*z* = 202.1807 ($C_{11}H_{24}NO_2^+$), *m*/*z* = 142.1590 ($C_9H_{20}N^+$). The detected NMR shifts are listed below:

^{1}H NMR (400 MHz, $CDCl_3$) δ: 3.73 – 3.51 (br m, 4H), 3.43 – 3.37 (br m, 2H), 3.13 (s, 3H), 2.22 – 2.11 (br m, 4H), 1.80 (s, 3H), 1.70 – 1.60 (br m, 2H), 1.40 – 1.27 (m, *J* = 36 Hz, 2H), 0.91 (t, *J* = 8 Hz, 3H).

^{13}C NMR (101 MHz, $CDCl_3$) δ: 176.6, 77.4, 63.9, 63.7, 48.1, 25.7, 25.4, 21.5, 19.7, 13.6.

Water content in as synthesized IL**A** was 4.44 wt% as determined by Karl Fisher (KF) coulometric titration (C20, Mettler Toledo).

Synthesis of IL**E**. A general synthesis procedure was taken from [59,60]. Detailed four-step synthesis of 1-poly(ethylene–glycol)-1-methyl-pyrrolidinium acetate (IL**E**) is shown in Scheme 2.

The first step (reaction 2) was preparation of compound **B** by tosylation reaction. A solution of alcohol (15 g, 0.043 mol), trimethylamine (8.67 g, 0.086 mol) and 4-dimethylaminopyridine (0.3 g, 0.025 mol) in chloroform (100 mL) was cooled to 0 °C (ice bath). Tosylchloride (12.26 g, 0.064 mol) diluted in chloroform (100 mL) was added dropwise and the solution was allowed to

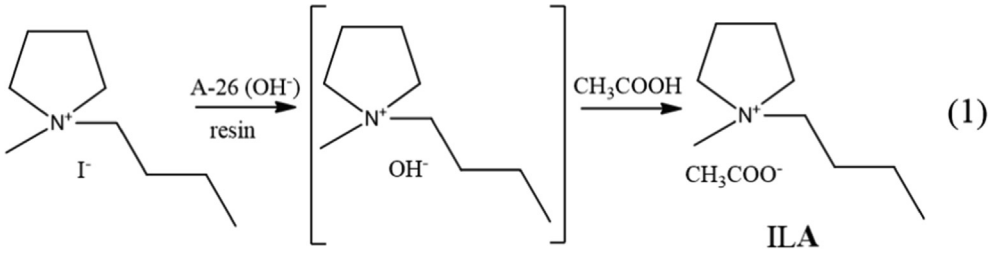

Scheme 1. Synthesis of [BMPyr]AcO (IL**A**).

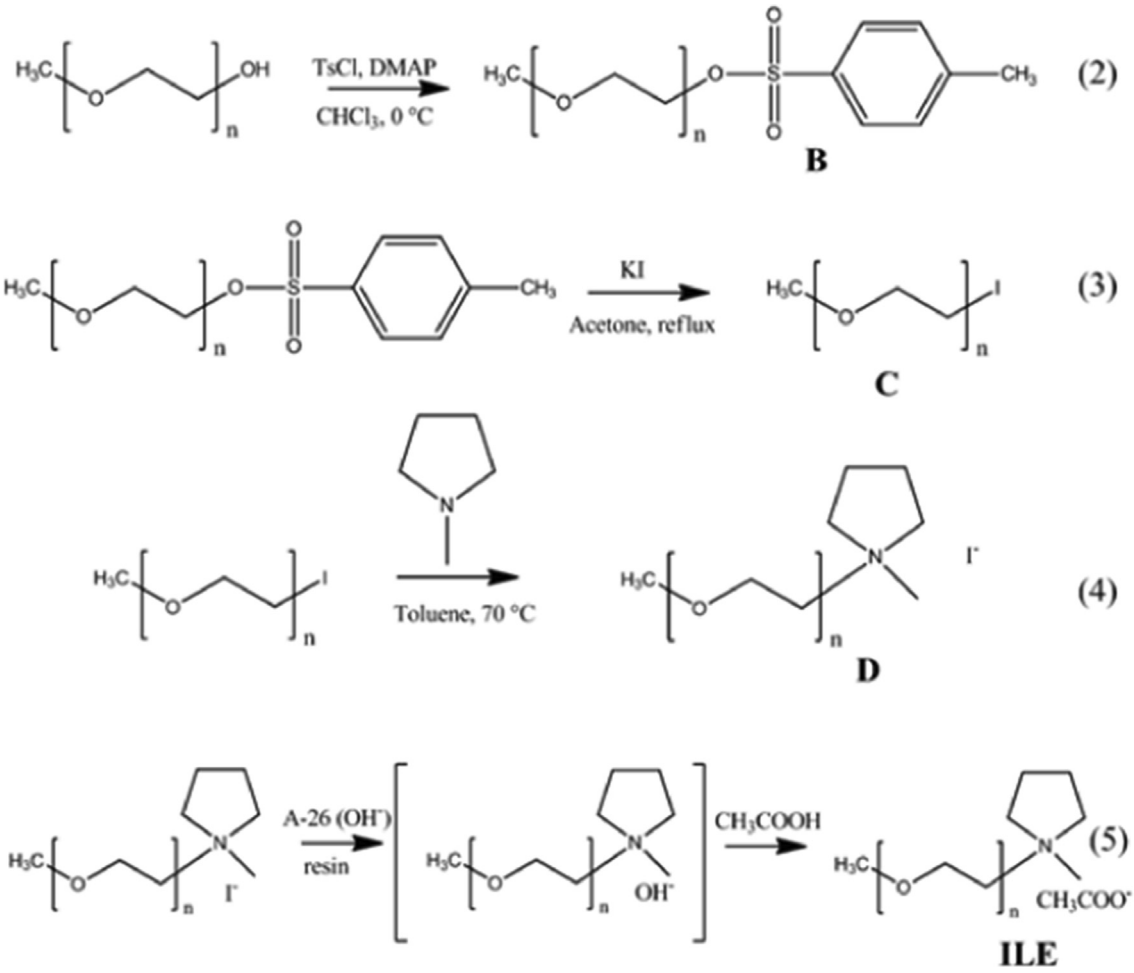

Scheme 2. Synthesis of [mPEG$_n$MPyr]AcO (IL**E**).

warm to room temperature under stirring for 12 hrs. Saturated $NaHCO_3$ (50 mL) was added and the solution was extracted, washed with H_2O (100 mL), dried over Na_2SO_4, and filtered. The solvent was removed under vacuum (rotary evaporator), and the crude product was purified by flash chromatography starting with cyclohexane/ethyl acetate (80/20) in order to eliminate the excess of 4-toluenesulfonyl chloride followed by dichloromethane/MeOH (90/10) to recover the pure tosylated alcohol (compound **B**) as a colorless oil: 17.73 g (82 % yield). The product was identified by ^1H, ^{13}C NMR and mass spectrometry. APCI (+) HRMS: major m/z = 495.2262 ($C_{22}H_{39}O_{10}S^+$).

^1H NMR (400 MHz, $CDCl_3$) δ 7.79 – 7.75 (d, J = 8 Hz, 2H), 7.34 – 7.29 (d, J = 12, 2H), 4.16 – 4.10 (br m, 2H), 3.67 – 3.64 (br m, 2H), 3.63 – 3.57 (br m, 19H), 3.56 – 3.54 (br m, 4H), 3.53 – 3.50 (br m, 2H), 3.35 (s, 3H), 2.42 (s, 3H).

^{13}C NMR (101 MHz, $CDCl_3$) δ 144.9, 133.1, 129.9, 128.0, 72.0, 70.8, 70.6, 69.3, 68.7, 59.1, 21.7.

The next step was the synthesis of compound **C** by nucleophilic substitution (3). Tosylated alcohol (17.73 g, 0.035 mol) was diluted in dry acetone (100 mL) and placed in a round bottom flask equipped with a refrigerating apparatus. Potassium iodide (11.62 g, 0.07 mol) was added and the system was placed in dark (aluminum foil). The solution was refluxed for 24 hrs. Resulting mixture was filtered through Celite, diluted with H_2O (100 mL), and extracted twice with CH_2Cl_2. Organic layer was dried over Na_2SO_4, filtered, and the solvent was evaporated under vacuum to give the iodide compound (12.62 g, 75 %) as a yellowish viscous oil (compound **C**) which was used without further purification. The later was identified by ^1H, ^{13}C NMR and mass spectrometry. APCI (+) HRMS: major m/z = 451.1189 ($C_{15}H_{32}O_7I^+$).

^{1}H NMR (400 MHz, $CDCl_3$) δ 3.73 – 3.67 (br m, 2H), 3.64 – 3.56 (br m, 21H), 3.52 – 3.47 (br m, 2H), 3.32 (s, 3H), 3.23 – 3.18 (br m, 2H).

^{13}C NMR (101 MHz, $CDCl_3$) δ 71.9, 71.9, 70.6, 70.6, 70.2, 59.0, 3.0.

Synthesis of compound **D** was made using quaternization reaction (reaction (4)). Iodide compound (12.62 g, 0,027 mol) and 1-methylpyrrolidine (2.52 g, 0,03 mol) were diluted in a round bottom flask and dissolved in toluene (100 mL). The mixture was stirred at 70 °C for 48 h. Two separated liquid layers were observed. The resulting $mPEG_nMePyrI$ salt was separated from toluene phase and washed with toluene (3 × 20 mL) and diethyl ether (3 × 20 mL). The residual product was successfully identified by ^{1}H, ^{13}C NMR and mass spectrometry as compound **D**. MALDI-TOF (matrix HCCA) (+) MS: major *m*/*z* = 408.29 ($C_{20}H_{42}NO_7^+$). MALDI-TOF (matrix DHB) (-) MS: *m*/*z* = 126.90 (I^-).

^{1}H NMR (400 MHz, $CDCl_3$) δ 3.99 – 3.85 (br m, 6H), 3.84 – 3.75 (br m, 2H), 3.69 – 3.63 (br m, 2H), 3.63 – 3.54 (br m, 19H), 3.53 – 3.47 (br m, 2H), 3.34 (s, 3H), 3.30 (s, 3H), 2.34 – 2.15 (br m, 4H).

^{13}C NMR (101 MHz, $CDCl_3$) δ 72.0, 70.6, 70.3, 65.8, 65.5, 63.3, 59.1, 49.4, 21.6.

Finally, IL**E** was obtained by anion exchange via reaction (5) (**Scheme 5.2**). Anion exchange reaction was realized as mentioned above for [BMPyr]AcO. Aqueous solution of $mPEG_nMePyrI$ (6.17 g, 0,011 mol) was passed through a chromatography column packed with 40 g Amberlyst A-26 hydroxide (OH^- form) dropwise. Equimolar amount of acetic acid (0.65 g, 0,011 mol) was added to the resulting solution. Neutral pH was controlled with pH meter Mettler Toledo. The water was carefully removed under vacuum using rotary vapor at 60 °C during for few hours. Absence of residual iodide was controlled by $AgNO_3$ test. The product was identified as $[mPEG_nMPyr]AcO$ (compound IL**E**) and by ^{1}H, ^{13}C NMR and mass spectrometry. APCI (+) HRMS: major *m*/*z* = 468.3149 ($C_{22}H_{45}NO_9^+$). Water content in as synthesized ILE was 2.73 wt% as determined by Karl Fisher coulometric titration.

^{1}H NMR (400 MHz, $CDCl_3$) δ 3.97 – 3.87 (br, 4H), 3.86 – 3.76 (br m, 2H), 3.72 – 3.63 (br m, 2H), 3.61 – 3.50 (br m, 23H), 3.49 – 3.43 (br m, 2H), 3.32 – 3.26 (m, 3H), 3.20 (s, 3H), 2.25 – 2.05 (br m, 4H), 1.85 (s, 3H).

^{13}C NMR (101 MHz, $CDCl_3$) δ 177.2, 77.2, 70.5, 70.4, 70.2, 70.1, 65.6, 65.1, 63.0, 59.0, 48.3, 25.4, 21.4.

2.1.3. RTIL identification

Mass-spectral analysis of the compounds **B**, **C** and IL**E** by MALDI-TOF mass-spectrometry was complicated by very close molecular mass values for some fragments and the composition of the initial alcohol ($mPEG_nOH$). Firstly, mass analysis of the initial $mPEG_nOH$ revealed that it exists as an extended population of monomers $(-CH_2-CH_2-O-)_n$, where n is in the range 4 < n < 14, with the difference of the molecular masses 44.0262 Da. Products **B** ($mPEG_nOTs$) and **C** ($mPEG_{n-1}I$) (scheme 2) differs hence by 0.0829 Da, hence, their distinguishing difficult. Thus, we provided an analysis by high resolution mass spectrometry (HRMS) with atmospheric pressure chemical ionization (APCI-Orbitrap), which allowed to identify correctly the formed reaction products.

2.2. Water - RTIL mixtures

Water-RTIL mixtures in a very large range of water concentration were studied both in the experiments and by modelling. For the experimental characterization the mixtures were prepared gravimetrically using freshly prepared Milli-Q water (18.2 $M\Omega{\cdot}cm^{-1}$) and "as synthetized" ILs in ratios shown in Tables 1 (**a**) and (**b**).

Table 1
Composition of water - RTIL mixtures studied experimentally or by modeling (marked by *).

(a) IL**A** – H_2O mixtures

Mass fraction of H_2O in IL**A**, ω(H_2O), %	Molar fraction of IL**A**	Molar fraction of water, χ(H_2O)	n(H_2O) / n (IL**A**)
0*	1*	0*	0*
4.44	0.658	0.342	0.519
6.25	0.573	0.427	0.744
8.22*	0.500*	0.500*	1.000*
8.23	0.500	0.500	1.001
12.05	0.396	0.604	1.530
14.96	0.337	0.663	1.964
15.19*	0.333*	0.667*	2.000*
16.92	0.305	0.695	2.274
20.87	0.253	0.747	2.945
24.70	0.215	0.785	3.663
31.46	0.163	0.837	5.126
35.92	0.138	0.862	6.259
41.77	0.111	0.889	8.010
46.17	0.095	0.905	9.578
50.00*	0.082*	0.918*	11.167*
51.45	0.078	0.922	11.834
54.63	0.069	0.931	13.446
56.41	0.065	0.935	14.451
64.92	0.046	0.954	20.665
74.84	0.029	0.971	33.216
84.11	0.017	0.983	59.108
94.78	0.005	0.995	202.754
100	0	1	–

(b) IL**E** – H_2O mixtures

Mass fraction of H_2O in IL**E**, ω(H_2O), %	Molar fraction of IL**E**	Molar fraction of water, χ(H_2O)	n(H_2O) / n (IL**E**)
0*	1*	0*	0*
2.73	0.574	0.426	0.742
4.30*	0.462*	0.538*	1.166*
4.55	0.447	0.553	1.237
5.04	0.421	0.579	1.377
6.25	0.336	0.634	1.730
8.24*	0.300*	0.700*	2.330*
8.43	0.295	0.705	2.388
9.53	0.268	0.732	2.733
11.47	0,229	0.771	3.361
12.93	0.206	0.794	3.853
15.09	0,178	0.822	4.611
17.96	0.150	0.850	5.680
20.90	0.127	0.873	6.855
21.22*	0.125*	0.875*	6.988*
23.43	0.112	0.888	7.939
26.36	0.097	0.903	9.316
26.42*	0.097*	0.903*	9.287 *
28.29	0.089	0.911	10.235
30.94	0.079	0.921	11.624
32.82	0.073	0.927	12.675
37.08	0,061	0.939	15.290
40.00*	0.055*	0.945*	17.296*
45.77	0,044	0.956	21.897
50.00*	0.037*	0.963*	25.944*
54.59	0.031	0.969	31.189
64.66	0.021	0.979	47.469
74.66	0.013	0.987	76.441
84.86	0.007	0.993	145.419
95.20	0.002	0.998	514.565
96.97	0.001	0.999	830.308
98.98	$4.000 \cdot 10^{-4}$	0.9996	2517.629
100	0	1	–

ω - mass fraction, %; χ - molar fraction.

2.3. Electrochemical characterization

The ionic conductivity of RTILs and of their aqueous mixtures was measured by the electrochemical impedance spectroscopy

(EIS) method using a Solartron Modulab potentiostat with ECS software interface in home-made dip-type conductivity cell having a cell constant of 3.78 ± 0.05 cm^{-1} with two parallel platinum electrodes at 10 mV amplitude vs E_{oc} within the frequency range 100 MHz – 100 Hz. The cell constant was determined by measuring the impedance of 0.01 M KCl aqueous solution (σ = 1.408 mS·cm^{-1} at 25°°C). All the measurements were conducted at least 5 times in a Faraday cage and at temperature 25 ± 0.2 °C.

Electrochemical potential windows (EPWs) of RTILs were investigated by cyclic voltammetry (CV) method using a Solartron Modulab potentiostat with ECS software interface in home-made three-electrode system. Glassy carbon disk (S = 0.0314 cm^2), Pt-wires and pseudo-AgCl/Ag electrode were used as working, counter and reference electrodes respectively. Pseudo-reference Ag/AgCl electrode was calibrated using 0.01 M $K_3[Fe(CN)_6]$. This calibration solution was selected because of the previously reported instability of ferrocene and its analogous in RTILs [61]. The potentials of oxidation/reduction pair of $K_3[Fe(CN)_6]$ were determined by Cyclic Voltammetry as $V_{(FeIII/FeII)}$ = −0.54 V and $V_{(FeIII/FeII)}$= −0.395 V in IL**A** and IL**E** respectively (see supplementary information **Fig. S1**). The measurements were conducted with the scan rate of 50 mVs^{-1}.

2.4. Chemical characterization by vibrational spectroscopy

Raman spectra were recorded with a Renishaw Confocal Raman Microscope InVia using red laser (HeNe, 633 nm, 17 mW power). The samples were deposited as a droplet (approximately 15 μl) on a support (Si-plate) and covered by a transparent microscope glass cover. Laser beam was focused on the liquid phase between the Si-plate and glass. The focus was reached using a microscope objective Leica of × 50 magnification and numerical aperture (NA) of 0.75. The exposure time was 10 s and 25 spectra were recorded for each sample.

Attenuated Total Reflection Fourier Transform Infrared (ATR-FTIR) spectra were recorded using Thermo Scientific Nicolet 6700 FTIR spectrometer equipped with a mercury cadmium telluride detector cooled at 77 K by liquid nitrogen. The ATR accessory was a horizontal ZnSe crystal coated with diamond (A = 2.54 mm^2) with single reflection and an angle of incidence of 45° (Smart Miracle from PIKE). The spectra were recorded with resolution 2 cm^{-1} and were averaged from 64 scans in order to minimize duration of the contact of samples with air and corrected by corresponding refractive index. Although some absorption of moisture from the air is possible during the measurement, we assume that its effect can be neglected if compared with the initial water content which was several wt. % even for the less concentrated in water samples (see Table 1). A droplet of the sample was placed on the diamond ATR crystal and the measurement started immediately, five spectra were recorded for each concentration. OMNIC software was used for the data collection and treatment. Further deconvolution of the spectra has been done using OriginPro 2018b using the following base line correction parameters: constant Y = 0; number of peaks: 4; fitting function: Gaussian; any other parameters were floating; R-square was higher than 0.999 for all fitted spectra.

2.5. MD modeling methodology

Gauss-View 6 was used for visualization [62] together with Gaussian 16 [63] for calculations in junction with the Antechamber module [64,65] to assign the Restrained Electrostatic Potential (RESP) charges for each atom. As the protocol requires, Gaussian structure optimizations were carried out at Hartree Fock level of theory with the standard 6–31* basis, as required by the RESP protocol [66].

We performed different simulations of one hundred pairs of IL cations and acetate anions, and an appropriate number of water molecules were added to reproduce desirable water concentrations. The molar water fractions $\chi(H_2O)$were 0.500, 0.667, 0.918 for IL**A** and 0.538, 0.700,0.875, 0.903, 0.954, and 0.963 for IL**E.** More detailed description of each mixture can be seen in **Supplementary information**, **Table S1**. The starting configuration were created with the PACKMOL package [67].

The MD simulations were carried out with the LAMMPS package [68,69]. The equilibration, 1 ns long or even more, was completed at ambient conditions (T = 298.15 K) in a canonical ensemble NVT with volume reflecting the real densities values found experimentally. Production runs, in a microcanonical ensemble NVE, were performed for at least 1 ns. The total energy drift ΔE_{tot} / E_{tot} was checked to be smaller than 10^{-6}.

Structural characterization was realized through the observation of radial distribution function, G(r), of the distance between the selected species. Its definition for the two α and β atoms types is given by the following formula:

$$G_{\alpha,\beta}(r) = \frac{1}{N_\alpha \cdot N_\beta} \langle \sum_{i,j}^{N_\alpha,N_\beta} \delta(r_{ij} - r) \rangle \quad (6)$$

where the ⟨…⟩ indicates the usual ensemble average, and δ(x) is the Dirac delta function, r_{ij} is the distance between an i- and j-atoms whereas N is the number of atom for the specie i in the sample box. Hydrogen bonds can be considered as strong if the distance between the oxygen of RTIL and hydrogen of water (O(IL)···H(H_2O)) is less than 2 Å, while weak hydrogen bonds are characterized by O(IL)···H(H_2O) distances up to 3 Å [70].

3. Results

3.1. Electrochemical potential window

To the best of our knowledge, although, some works with $mPEG_n$-*N*-methylpyrrolidinium ILs were carried out [55], the experimental electrochemical stability of this cation, especially with acetate anion, has never been studied. Fig. 1 shows voltammograms of as synthesized ILA and IL**E** (molar fraction of water 0.342 and 0.426 in ILA and IL**E** respectively). Determined from these polarization curves the electrochemical potential windows

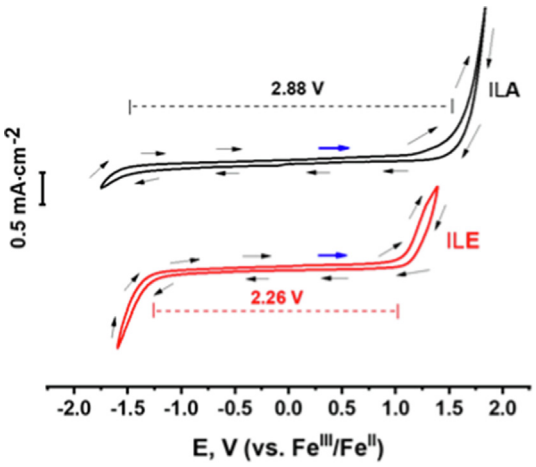

Fig. 1. Cyclic voltammograms recorded on glassy carbon disk electrode of "as synthetized" IL**A** and IL**E**, as indicated. Arrows indicate potential scanning direction starting from the blue one. Scan rate 50 mVs^{-1}. Electrochemical potential window is also shown by dash lines; the limits are determined at 0.1 mA·cm^{-2} current density cut off. (For interpretation of the references to colour in this figure legend, the reader is referred to the web version of this article.)

are: EPW≈2.26 V for IL**E** and EPW≈2.88 V for ILA. Especially, for IL**E** the EPW is narrowed at cathodic (negative) potentials. Such a difference in the EPW of two ionic liquids can be explained by the lower electrochemical stability of etheric bonds in substituted tail compared to the alkyl group because of their electrochemical reduction [71]. Similar effects have been previously reported for phosphonium and piperidinium cations [16,72–74]. The difference between the oxidation potentials of ILA and IL**E** remains unclear.

3.2. Specific conductivity

Specific conductivity of the electrolytes is one of their key-properties for the electrochemical applications. In some works, it has been shown that dilution of ILs by conventional electrolytes increases conductivity [12,17,75]. Fig. 2 represents specific conductivity (σ, mS·cm^{-1}) of water - ILA and water - IL**E** mixtures as a function of the water content (molar fraction). As it can be seen from the figure, the conductivity of the ILA is systematically higher than that of the IL**E**, which can be explained by a shorter length of the substituted tail resulting in higher ionic mobility. Another hypothesis explaining this difference can be that a relatively high-donor and low-acceptor numbers of etheric group can result in agglomeration of the cations by the electron - ion pairs thus reducing ionic conductivity, as was observed for (triglyme): LiX (X = $CF_3SO_3^-$, BF_4^-, ClO_4^-, and AsF_6^-) systems [76]. The conductivity increases with the water content and has a maximum of 27.9 ± 0.1 mS·cm^{-1} at χ (H_2O) = 0.971. On the contrary, for the IL**E** the maximum of specific conductivity is observed at χ (H_2O) = 0.987 with the only at 11.0 ± 0.1 mS·cm^{-1} which is more than two times lower than for the ILA. Conductivity growth with dilution can be explained by three factors: a) viscosity decrease which leads to a higher mobility of ions; b) formation of water clusters which allow ions to move freely [77,78] and c) decrease of cations agglomeration because of their coordination with water molecules [76]. Since, ILA and IL**E** have the same anion (acetate), the substituted chains at nitrogen atoms play a crucial role in the conductivity evolution. Sharp decrease of conductivity at very high water contents is similar to the expected for diluted aqueous solutions in which only isolated hydrated ions ensure conductivity, so less is the fraction of ions, lower conductivity. One could consider hence that starting from the concentration corresponding to the maximal conductivity, the interactions between IL ions could be neglected if compared with the interactions with water molecules.

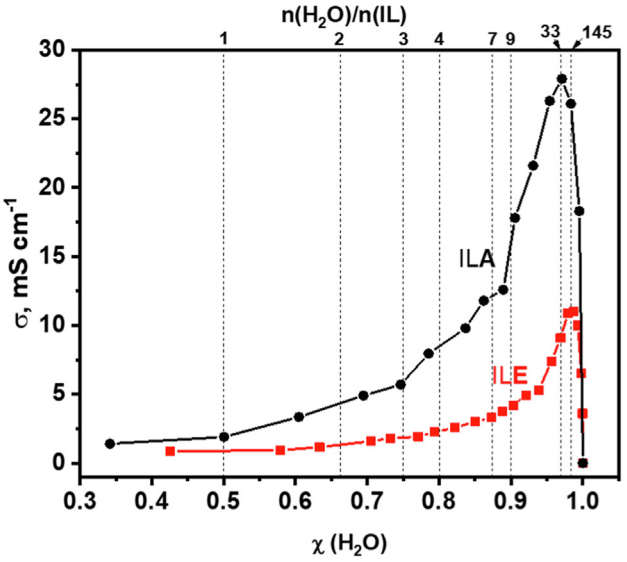

Fig. 2. Specific conductivity of water-IL**A** and water-IL**E** mixtures, σ, as a function of molar water content χ(H_2O). Vertical lines show fractions for some selected molar ratios between water molecules and IL molecules n(H_2O)/n(IL) as indicated.

The difference between the two ILs becomes even more visible if not the molar fraction but the ratio between the number of water molecules and the number of the IL ions pairs, n(H_2O)/n(IL), is considered as it is indicated on the top axis. It is clear in this consideration that not only the maximal conductivity is significantly higher for IL**A** but also the maximum is achieved for about 4–5 times smaller number of water molecules per one molecule of IL (33 for the IL**A** and 145 for the IL**E**) which indicates very different water availability for the structure typical for that observed in aqueous solutions (water with isolated solvated ions).

3.3. Raman spectroscopy of water-RTIL mixtures

Fig. 3 displays typical Raman spectra of water-RTIL mixtures for ILA (**a**) and IL**E** (**b**) as a function of water content. The detailed attribution of the peak positions can be found in Supplementary information (Table S2). As it can be seen from Fig. 3 **(a),** the Raman peaks at 637, 906, 1325, 1387 cm^{-1} shift to higher wavenumbers with increasing of water content. These peaks are usually attributed to acetate anion vibrations [79]. The band nearby 905 cm^{-1} on the spectra of the ILA **(a)** and the IL**E** **(b),** containing 0.342 and 0.426 water molar fraction respectively, consists of two peaks attributed to pyrrolidinium ring [80] and acetate anion which are not distinguishable. Growth of the water content leads to the formation of a shoulder and then to the bifurcation of the peak. The second peak nearby 914 cm^{-1} appears at χ(H_2O) = 0.747 and χ (H_2O) = 0.794 for the ILA and the IL**E** respectively. These observations indicate that water molecules strongly interact with acetic group in both ionic liquids, which is coherent with the previously reported results [81–83]. For the IL**E** (Fig. 3 **b**), the spectra evidence not only the interactions of water with the anion, but the form of the broad band, ascribed to the stretching of C—O—C group in PEG chain (770–867 cm^{-1}) also evolves. If the band maximum was nearby 826 cm^{-1} at the lowest concentration of water its position moves with dilution resulting to the maximum peak position shift up to nearby 850 cm^{-1}. This can be attributed to the interaction between water and PEG via etheric group, leading to conformation changes in the etheric group and PEG chain [84,85]. One could also note in the figure, that a relative height of etheric band, if compared for instance with the neighboring acetate band at 905 cm^{-1}, increases with dilution by water. This suggests stronger polarizability of C—O—C group which could for instance result from the bond length increase by the interactions between etheric oxygens and water.

3.4. ATR-FTIR spectra of water-RTIL mixtures.

Fig. 4 **(a, b)** displays ATR-FTIR spectra of IL**A** and IL**E** within the range of 750–3800 cm^{-1}. All the peaks attributions are shown in the supplementary information (**Table S3**). It is obvious from Fig. 4 that the higher the water content is, the higher the O—H absorbance peaks (3000–3700 cm^{-1}) and the lower the peaks corresponding to the ILs absorbance are. Similar to Raman spectra, positions of some peaks change with dilution. As can be seen from Fig. 4 **b**, peaks nearby 1379 cm^{-1} and 1583 cm^{-1} suffer blue and red shifts respectively. These peaks are attributed to C—O and C—H vibrations of acetic groups [82,86]. It should also be noted that on the spectra of the IL**E** these shifts are also observed. Less intensive peaks, attributed to acetic groups nearby 906 cm^{-1}, 1004 cm^{-1}, 1323 cm^{-1} and 904 cm^{-1}, 1325 cm^{-1} for IL**A** and IL**E** respectively (indicated in Fig. 4), are also shifted. For water - IL**E** mixtures, the positions of the peaks around 1107 cm^{-1} and

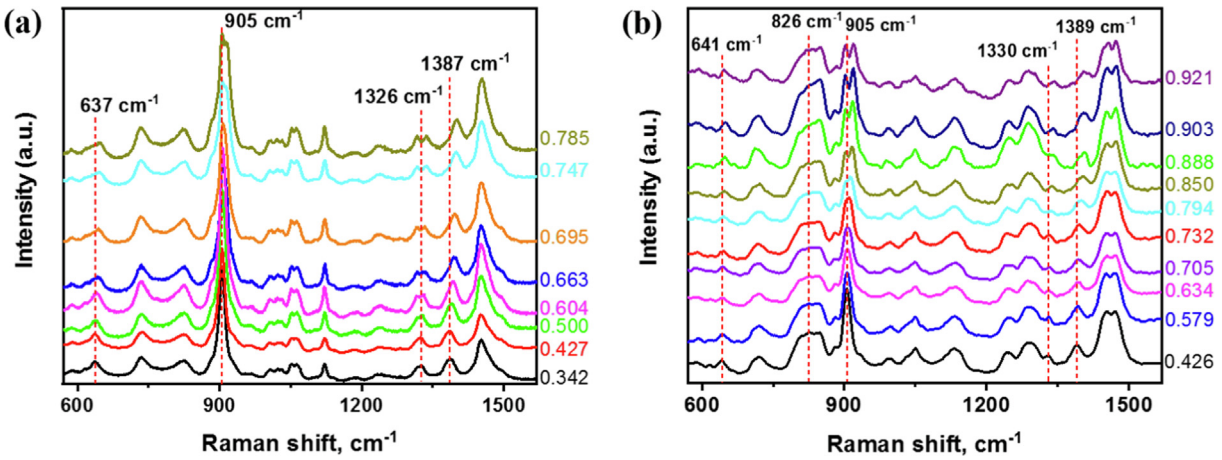

Fig. 3. Typical Raman spectra of water mixtures with IL**A** (**a**) and IL**E** (**b**) with different molar fractions of water (as indicated at right of each spectrum). All noted bands positions in **(a)** are attributed to vibrations of AcO^- anion. In (b), the peaks with similar positions are also ascribed to AcO and the broad band near 826 cm^{-1} is attributed to C—O—C vibrations of etheric groups in mPEG.

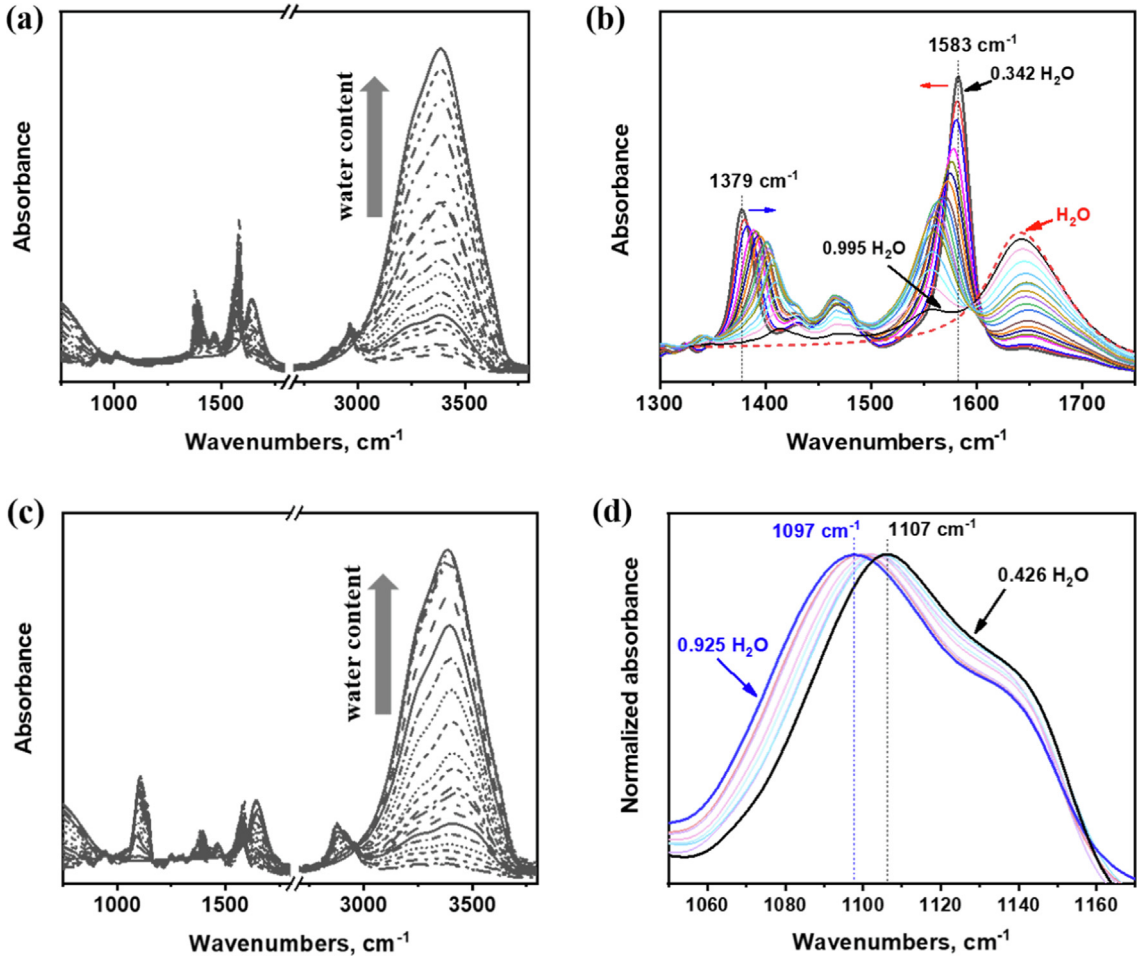

Fig. 4. Evolution of ATR-FTIR spectra for water – IL mixtures for IL**A** (a, b) and IL**E** (c, d) as a function of water content, with zoom on COO^- (**b**) and -C—O—C- (**d**) regions. Shown water molar fractions $\chi(H_2O)$ are: **(a, b)** 0.342, 0.427, 0.500, 0.605, 0.663, 0.695, 0.747, 0.786, 0.837, 0.862, 0.889, 0.905, 0.922, 0.931, 0.954, 0.971, 0.983, 0.995, 1 (pure water); **(c)**: 0.426, 0.553, 0.579, 0.634, 0.705, 0.732, 0.794, 0.873, 0.888, 0.903, 0.911, 0.939, 0.956, 0.969, 0.979, 0.987, 0.993, 0.998, 0.999, 0.9996, (pure water);**(d)**: 0.426, 0.705, 0.794, 0.850, 0.873, 0.903, 0.911, 0.925.

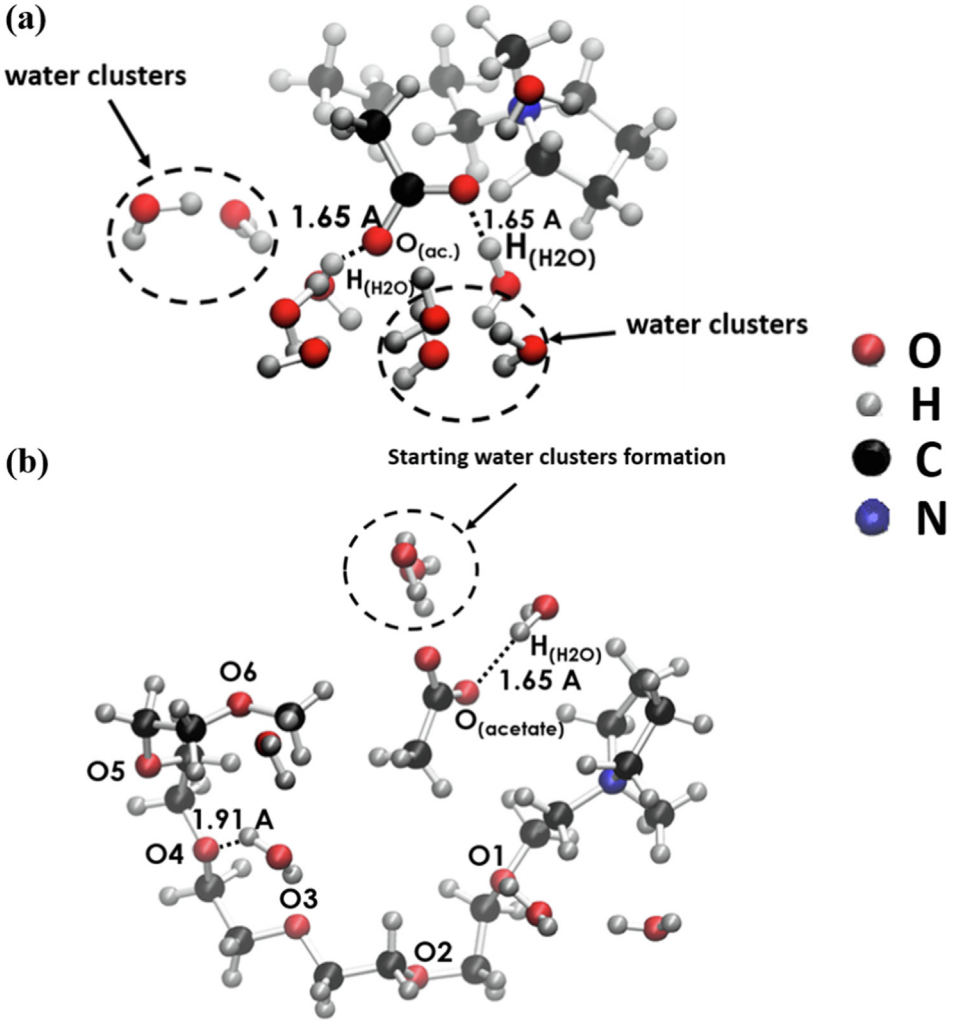

Fig. 5. Representation of models IL**A** containing $\chi(H_2O)$ = 0.918 ($n(H_2O)$ / n(IL**A**) ≈ 11) – (**a**); IL**E** model representation $\chi(H_2O)$ = 0.903 ($n(H_2O)$ / n(IL**E**) ≈ 9) – (**b**).

1248 cm^{-1}, attributed to C—O—C etheric group [52], also shift with dilution (Fig. 4 **d**).

3.5. Radial distribution function for hydrogen bonds in water - RTILs mixtures from MD simulation

Fig. 5 represents the example of typical configurations of ILs molecules with the closest water molecules, extracted from the MD calculations for the models with approximate water molar fraction $\chi(H_2O)$ = 0.918 for IL**A** and $\chi(H_2O)$ = 0.903 for IL**E**. The closest distances between the water hydrogen atoms and acetate hydrogen atoms are indicated. Oxygen atoms numbering in etheric groups is also shown (the distance for O4···H_2O is indicated). The shortest distances between water H-atoms and O atoms of the IL are also indicated. Normally a distance between O and H atoms smaller than 3 Å is attributed to the formation of a hydrogen bond [70]. The results shown in Fig. 5**a-b** thus indicate the formation of H-bonds between water and acetate anion and also etheric oxygens in case of the IL**E**. In the model with the IL**A**, water clusters are formed at this concentration. In contrast, the model with the IL**E** shows only some embryos of water-clusters formations.

These extracted structures are however only illustrative, a more quantitative description of H-bonding can be obtained analyzing the radial distribution function (RDF), G(r). The G(r) graphs (see Figs. 6, 7) describe the probability of finding a hydrogen atom of a water molecule at a distance r (measured in Å) from the selected oxygen. Due to dynamical movement, liquids do not maintain a constant structure, so at large distances the molecules are independent and the distribution returns to the bulk density (G(r) = 1). However, at short distances the first peak indicates the first coordination sphere, so the existence of a specific interaction between atoms, e.g. H-bonds between acetate anion, $O_{acetate}$, and water hydrogen atom H_{H2O}, is revealed by a specific peak at short distance in the radial distribution function $G(O_{acetate}/H_{water})$. Fig. 6 **(a) and (b)** represent the $G(r_{Oacetate\cdots Hwater})$ for the distance between the acetate oxygen and water hydrogen in the IL**A** and the IL**E** mixtures with different water contents. They are characterized by two peaks nearby 1.65 Å and 2.97 Å. It is clear from the figure that the intensity of both peaks decreases with dilution, indicating that the probability to find a water molecule H-bonded with an acetate anion rapidly decreases for both ILs with increasing water concentration. As a consequence, the probability to find a water molecule not H-bonded with an acetate anion increases.

The $G(r_{O(etheric)\cdots H(water)})$, representing the length distribution between the etheric oxygen and the hydrogen of water also revealed two peaks but nearby 1.92 Å and 4.90 Å (see an example on Fig. 7, on the schematic representation only the attribution of the peak at ≈1.92 Å is shown). It can be seen from the figure that the effect of the dilution on the probability that water molecule added to the mixture will be H-bonded with the selected etheric oxygen (O4) increases with dilution.

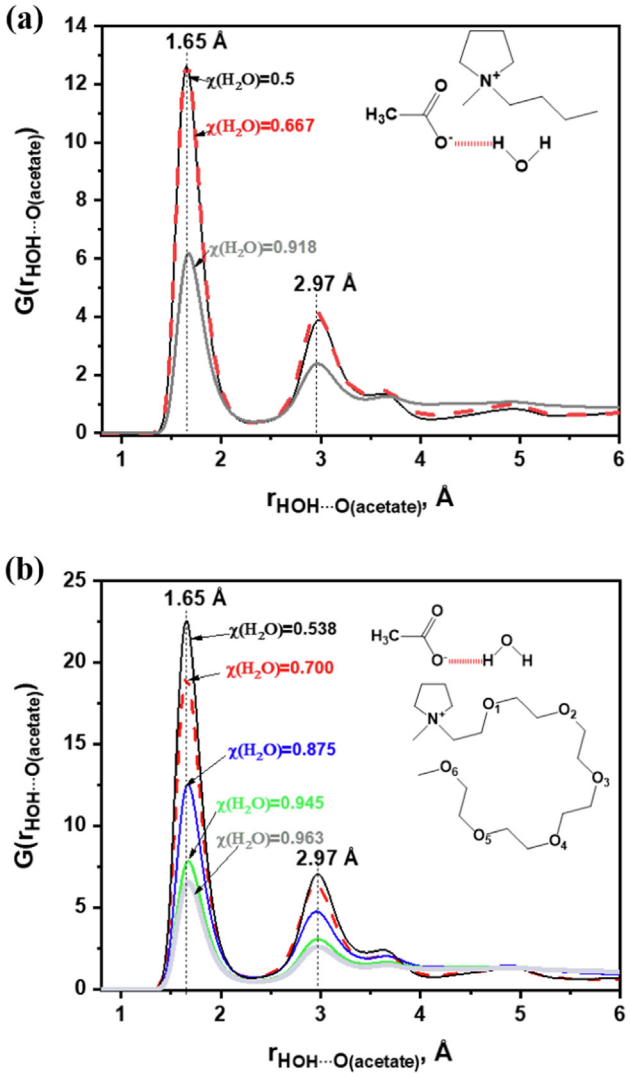

Fig. 6. Radial distribution function $G(r_{HO\text{-}H\cdots O(acetate)})$ of the distances between water hydrogen and acetate oxygen, $r_{HO\text{-}H\cdots O(acetate)}$, for selected H_2O - IL**A** (**a**) and H_2O - IL**E** (**b**) mixtures. Water molar fractions $\chi(H_2O)$ are indicated.

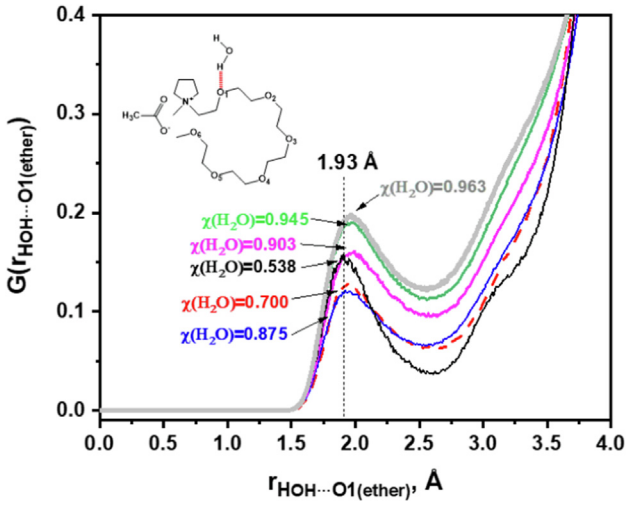

Fig. 7. Radial distribution function $G(r_{HO\text{-}H\cdots O(etheric)})$ of the distances between water hydrogen and the first etheric oxygen, $r_{HO\text{-}H\cdots O(etheric)}$, for water mixtures IL**E** with selected water molar fractions $\chi(H_2O)$ as indicated.

The effect of water content in the mixture on the height of the peak in the G(r) functions, describing the probability of H-bonding between H-atom from water with O atom of the selected group, is presented in Fig. 8 (for the acetate groups of the ILA and the ILE) and Fig. 9 (for different etheric oxygen atoms of the IL**E**). Comparing Fig. 8 and Fig. 9 suggests that upon dilution the probability to find a water molecule H-bonded with acetate decrease for both ILs, however the probability that it is H-bonded to the etheric oxygen increases. This can be interpreted as for the IL**A**, which does not contain etheric oxygen in the cation, "free" water clusters are expected to appear rapidly. This "free" water is not expected immediately for the IL**E** because although the probability of water bonding with acetate decreases, in place of being "free", water molecules can be H-bonded to etheric oxygen atoms of the PEGylated cation.

Interestingly, different etheric oxygen atoms show different intensities of the first peak (Fig. 9), indicating different probability

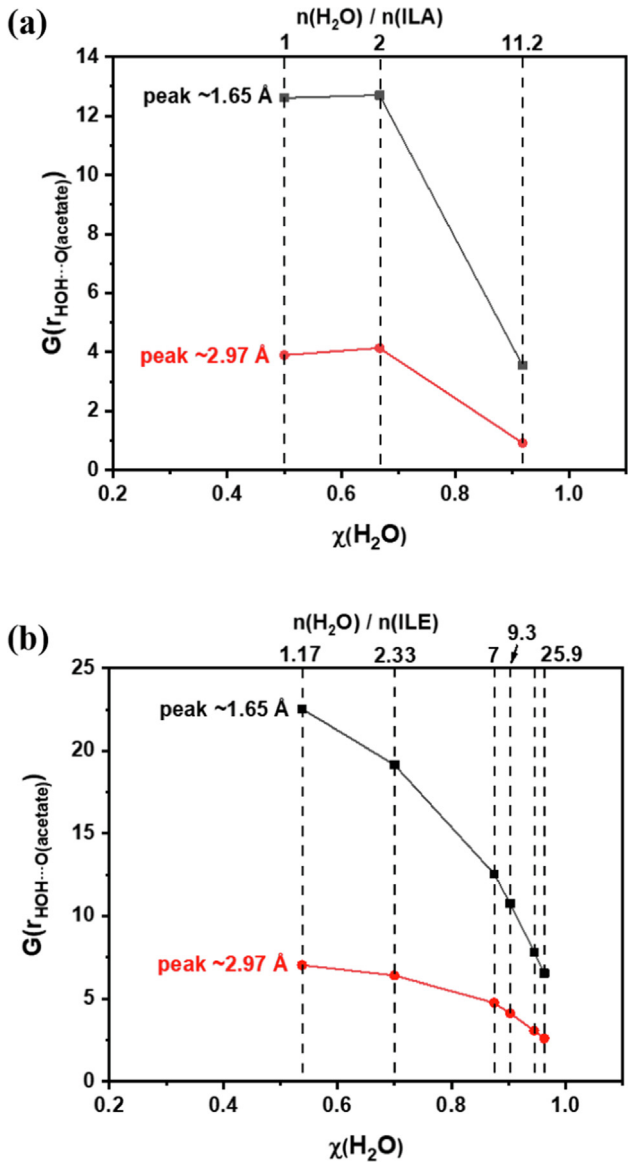

Fig. 8. Evolution of the intensities of the first two peaks of RDF for the distances $r_{HO\cdots O(acetate)}$ between the hydrogen from water and the oxygen from the acetate anion as a function of water molar fraction in water mixtures with IL**A** (a) and IL**E** (b). Vertical dash lines indicate selected molar ratios of water to ILs, $n(H_2O)$ / n(IL**A**) and $n(H_2O)$ / n(IL**E**), as indicated.

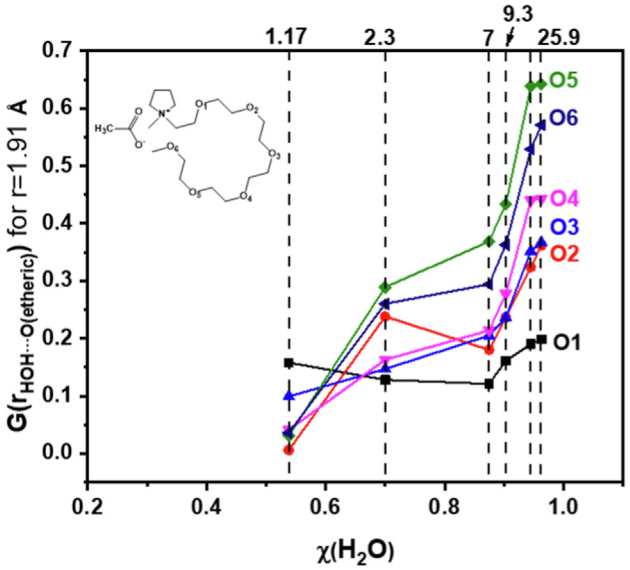

Fig. 9. Evolution of the peak intensity of $G(r_{HO\text{-}H\cdots O(etheric)})$ at $r_{HOH\cdots O(etheric)}$ = 1.93 A for ILE-H_2O mixtures with selected H_2O molar fractions $\chi(H_2O)$. Vertical dash lines indicate some selected molar ratios of H_2O to IL**E**: $n(H_2O)$ / n(IL**E**).

of H-bonding between this oxygen and water. At concentration $\chi(H_2O)$ = 0.538 the highest intensity of the RDF characterizing the length of $H_{(water)}\cdots O_{(etheric)}$ bonds is observed for O1 and O3 (counting from N^+). This is the minimal studied water content, at which the probability of H-bonding between water molecules and acetic group is also the highest (Fig. 8 **b**). Thus, it can be assumed that a significant fraction of water is confined between acetate and etheric oxygens (O_1, O_3), forming $AcO\cdots HOH\cdots O_{(etheric)}$ segregations, which are sterically the closest to acetate. This is also supported by the fact that the RDF intensities of HO-H···O1(etheric) does not change significantly with water fraction in the mixture (Fig. 9).

Another interesting observation is a rapid increase of the RDF intensities.

$O_{(etheric)}\cdots$H-OH for all other oxygens (O2 - O6) for water fractions $\chi(H_2O)$ = 0.875 and higher. This might indicate the start of "free" water - clusters formation.

Thereby, in function of the water content in the water – IL**E** mixtures, the water state in the liquid can be attributed to one of the structures described below. Within the first concentration region ($\chi(H_2O)$ = 0.442 – 0.702) water molecules are supposed to be strongly H-bonded to acetate moieties (AcO···HOH···OAc). In the second concentration range ($\chi(H_2O)$ = 0.702 – 0.872) the mixture is characterized by the existence of hydrogen bonds AcO···HOH and $O_{(etheric)}\cdots$HOH. Water clusters are expected to be present and to continuously grow in the water – IL**E** mixtures with water content $\chi(H_2O)$ = 0.872 and higher. For the water – ILA mixtures the second concentration range (with water bonded to etheric oxygen) is impossible, growth of water clusters is expected hence at much lower water content. All of these conclusions were supported by dynamic boxes, in which the appearance water-clusters was clearly observed for significantly lower water contents in mixtures with the ILA than with the IL**E** (supplementary information **Table S4**).

4. Discussion

4.1. Effect of water content on molecular structure of water-RTIL mixtures for aliphatic and etheric substituted $[MPyr]^+AcO^-$ RTILs

In order to understand water state in various solutions, the literature suggests to explore the evolution of infrared spectra in the region of O—H vibrations (3000–3700 cm^{-1}) [44,87–90]. Fig. 10 compares the spectra of pure water with the spectra of water-ILA and water-IL**E** mixtures in the close to 1:1 water to IL molar ratio (molar water fraction $\chi(H_2O)$ = 0.427 and $\chi(H_2O)$ = 0.426 for ILA and IL**E** respectively). For both mixtures the peak's width at half-height is smaller than for pure water, which evidences that water molecules are separated from each other [87]. Additionally, in the water-IL**E** mixture but not in water-ILA mixture an additional shoulder appears at nearby 3757 cm^{-1} (Fig. 10). This additional vibration peak at 3757 cm^{-1} can be tentatively explained by the suggested from the MD simulation structures in which water is confined between acetate and etheric oxygens (O_1 or O_3), forming $AcO\cdots HOH\cdots O_{(etheric)}$ segregations, which are sterically the closest to acetate (see section **3.5**).

To quantify the evolution of the molecular structure, the spectra of all mixtures were reproducibly decomposed into four single Gaussian functions (A, B, C, D), as illustrated on the examples shown in Fig. 11 **a, b**. Unfortunately, there is no unique model describing the water band decomposition in solutions, in different works it is decomposed into 3, 4 [91,92]; 5 or 6 bands [44,90,93]. In theory, hydrogen bonding should decrease vibrational mobility of H-atom, so the vibration frequency modifications and peak splitting can be expected. Although the decomposition of water band into individual components and attribution of their vibration wavenumbers requires multiple "a priori" even for pure water [92], in the present work we have chosen an empirical four-component decomposition which fitted well for all the studied spectra.

Peaks A and B in Fig. 11 correlate with the positions attributed in the literature to a "network water" (continuous water cluster) and an "intermediate water" (finite clusters), respectively [93]. According to other work [94], peak A can be considered as representing the O—H vibration of water phase not interacting with IL anions, while peak B can be associated with the OH-vibration of the water molecules interacting with the RTIL anions. In both interpretations ([93,94]) it seems that comparing contributions of peaks A and B for different water contents one can evaluate the evolution of the water state in the mixture. Relatively high peak B could indicate that water molecules are mostly associated with ion pairs of IL or representing solvation shell, whereas high peak A represents water molecules which interact with other water molecules.

The signals at high frequencies (peaks C, D) could be attributed to "dangling" OH groups of "multimers" (dimers and trimers) [93]. The contribution of peak D is however near 0 for all water contents

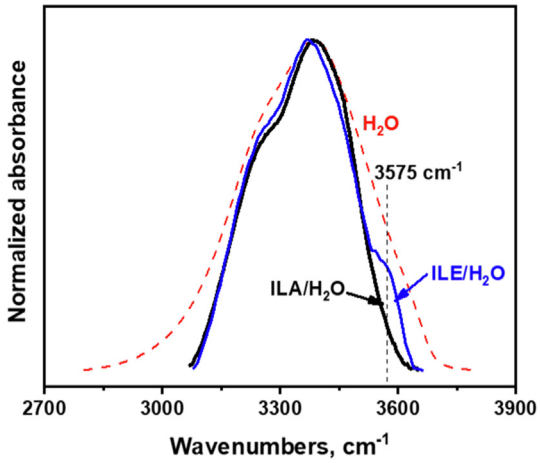

Fig. 10. FTIR spectra of IL**A** ($\chi(H_2O)$ = 0.427) - black, IL**E** ($\chi(H_2O)$ = 0.426) – blue, and pure H_2O – dash red line. (For interpretation of the references to colour in this figure legend, the reader is referred to the web version of this article.)

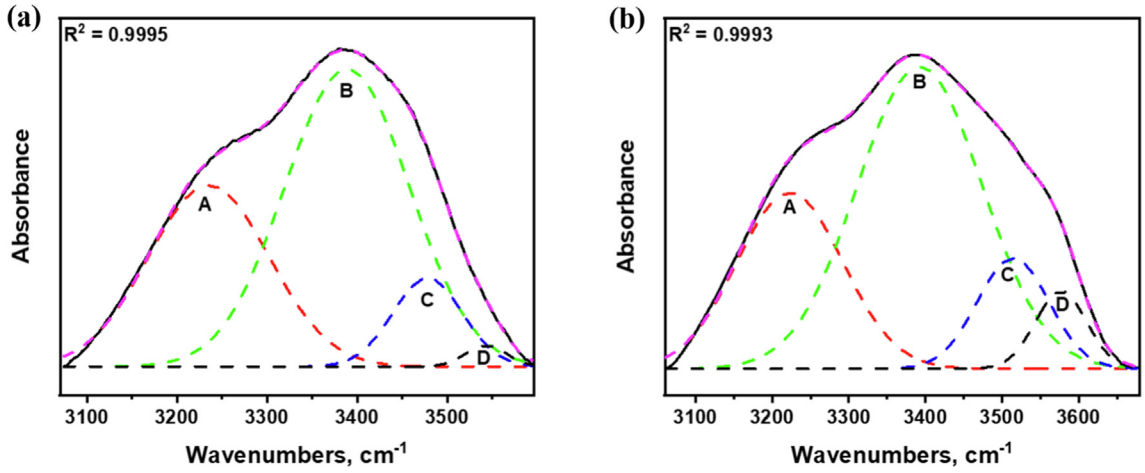

Fig. 11. Typical decomposed FTIR spectrum of IL**A** containing ($\chi(H_2O)$ = 0.427) – **a**, IL**E** containing ($\chi(H_2O)$ = 0.705) – **b**.

in the ILA – water mixtures. In contrast, for the mixtures containing the IL**E**, its contribution becomes stronger. In coherence with the results of MD simulation suggesting interaction between etheric oxygen and water molecules (section 3.5) and with the systematic shifts of C—O—C Raman and infrared peak positions with addition of water to IL**E**, peak D for the IL**E** was assigned to weak H- bonds between water molecules and etheric oxygens of the PEG-cations.

Fig. 12 displays the results of the decomposition of water bands, in which the area fraction of each peak (A, B, C and D) is shown as a function of molar water fraction in the water mixtures with IL**A** (Fig. 12 **a)** and IL**E** (Fig. 12 **b)**. Additional top x-axis represents the ratio between the molar concentrations of water and ILs, which is useful to compare experimental and modelling results. As can be seen from the figure, at least 2 regions can be noticed for IL**A**. At water molar fractions below $\chi(H_2O)$ = 0.747, corresponding to the ratio of $n(H_2O)$ / n(IL**A**) = 3, the contributions of all the peak areas A-D do not change and are very different from the contributions detected for pure water ($\chi(H_2O)$ = 1). This indicates similar water state for all water-IL**A** mixtures where not more than 2 water molecules per one acetate ion are present ($n(H_2O)$ / n (IL**A**) = 2) and probably even for the first water molecule at the second sphere bounded to these.

AcO-HOH structures ($n(H_2O)$ / n(IL**A**) = 3). This is coherent with formation of hydrogen bonds considering acetate anion as monodentate (for the ratio $n(H_2O)$ / n(IL**A**) = 1) or bidentate (for the ratio $n(H_2O)$ / n(IL**A**) = 2) Lewis base. Similar results were already reported for imidazolium-based acetate ILs [41]. For higher water concentrations the peak A contribution becomes visibly higher and stays more or less constant up to enough big water contents. In this domain, the acetate ions are expected to be already saturated by water so they cannot form new H-bonds. This should lead to water clustering in which the interaction between water and acetate should pass through more than one sphere (AcO···H-OH···HOH···OH_2) making the behavior of water molecules far from the acetate similar to that in "free" water. Finally, for molar water fractions $\chi(H_2O)$ greater than 0.85 the peak A strongly increases and peak B decreases, both rapidly reaching the contributions similar to the measured in pure water, indicating that the mixture can be considered as an aqueous solution with a percolating water cluster and isolated hydrated organic ions.

It seems hence that the evolution of the IR peaks contributions reflects the evolution of the water structure in the mixture: bound water for molar ratios of water and ILA up to 2, water clusters for ratios starting from 3 to 4 and transition to isolated IL ions in

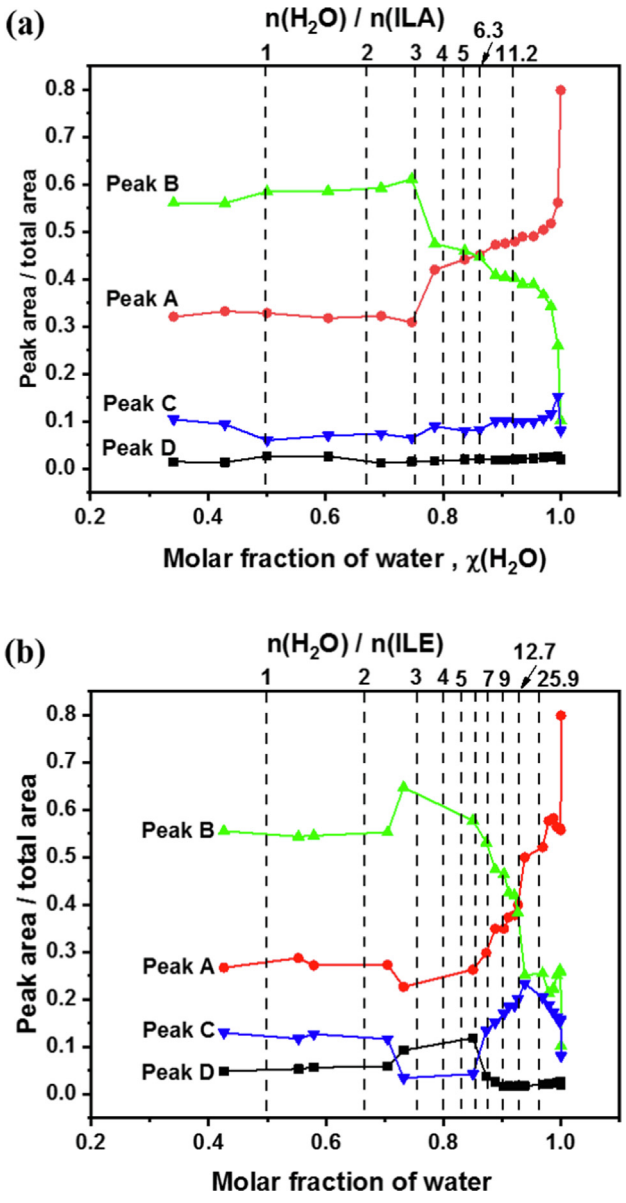

Fig. 12. Ratio of area of decomposed bands to total area as a function of water content for IL**A** – **a**, IL**E** – **b**.

aqueous solution for water molar fractions higher than 0.85. These speculations are supported by the discussed in section 3.5. evolution of the RDF for the H_{H2O}-$O_{acetate}$ distance (Fig. 8 **a, b**), showing significant loss of the probability to find a H-atom in the vicinity of O(acetate) with dilution.

Application of a similar approach to the water-IL**E** mixtures reveals some interesting observations. The increase of the contribution of the peak A starts only after the molar ratios n(H_2O) / n (IL**E**) higher than 7, indicating that the formation of water clusters in the IL**E** requires significantly higher water content. Interestingly, in the domain of molar ratios n(H_2O) / n(IL**E**) between 3 and 7 the contribution of the peak D, attributed to the presence of AcO···HOH···$O_{(etheric)}$ structures, increases about twice times and after this it decreases to zero. This is coherent with the idea that once the acetate anion is saturated with water, the excess water molecules are still bounded with IL, in this case with the cation via etheric oxygen. Such a bonding reduces the probability of water clustering, and hence "free" water phase formation and its mobility.

MD simulations illustrate different possible structures expected for selected water contents in the IL**A** and the IL**E** as can be seen in dynamic boxes and RDF results (see supplementary information **Table 4S**). Indeed, both, the first water pockets and the percolating water clusters appear at higher water contents for water-IL**E** mixtures.

To sum up, based on the experimental and theoretical (MD simulation) results obtained in this work, Table 2 represents probable water molecules organization in the water-ILs solutions.

4.2. Molecular structure of water-RTIL mixtures and their conductivity

The proposed speculative model of water organization in mixtures with the IL**A** and the IL**E** fits well with the observed in Fig. 2 specific conductivity evolution. Indeed, the conductivity increase with water content starts earlier and grows quicker for the IL**A** than for the IL**E**. The switch to the conductivity decrease with water addition also arrives earlier and the decrease is much sharper for the IL**A** than for the IL**E**. At water to IL molar ratios lower than 3 for IL**A** and lower than 7 for the IL**E**, all water molecules can be H-bonded to IL cations and anions. Ionic mobility is therefore limited and conductivity variation is expected to be very small. For higher water to IL ratios "free" water pockets start to appear, which are more mobile, less viscous and that can also transport acetate ions. This is expected to increase conductivity. Finally, at water to IL ratios of 33 (and higher) for the IL**A** and 145 (and higher) for the IL**E,** the solutions can be considered as diluted aqueous solutions in which hydrated IL anions ensure the charge transport.

Table 2
Water organization in water - IL mixtures with IL**A** (**a**) and IL**E** (**b**).

(a) ILA- H_2O	
n(H_2O) / n (IL**A**) = R (molar fraction, χ)	**Liquid structure**
$R \leq 2$ ($\chi(H_2O) \leq 0.69$)	IL + isolated water molecules H-bonded to AcO^-
$2 < R \leq 3$ ($0.69 < \chi(H_2O) \leq 0.74$)	IL + isolated H_2O molecules H-bonded to AcO^- directly or via only one water molecule
$3 < R < 33$ ($0.74 < \chi(H_2O) < 0.97$)	IL + isolated H_2O molecules H-bonded to AcO^- + "free" water clusters in IL
$33 \leq R$ ($\chi(H_2O) \leq 0.97$)	Percolating H_2O cluster + isolated IL ions
(b) ILE- H_2O	
n (H_2O) / n (IL**E**) = R (molar fraction, χ)	**Liquid structure**
$R \leq 3$ ($\chi(H_2O) \leq 0.75$)	IL + isolated water molecules H-bonded to AcO^-
$3 < R \leq 7–8$ ($0.75 < \chi(H_2O) < 0.86$)	IL + isolated water molecules H-bonded to AcO^- and PEG
$9 < R < 145$ ($0.90 < \chi(H_2O) < 0.99$)	IL + isolated water molecules H-bonded to AcO^- and PEG + "free" water clusters in IL
$R \leq 145$ ($\chi(H_2O) \leq 0.99$)	Percolating H_2O cluster + isolated IL ions

The origin of the difference between the water behavior in mixtures with the IL**E** and the ILA can be explained by the water coordination with etheric oxygen atoms. The latter was confirmed by the growth of the peak D fraction in the infrared spectra for water to IL**E** molar ratios between 3 and 7 (Fig. 12) and by the calculated increase of the probability of H-bonds between water and etheric oxygen (Fig. 9). Considering bidentate acetate anion, for molar water to IL ratios up to 2 ($\chi(H_2O)$ = 0.500–0.667) water molecules should be strongly bonded to acetate moieties (AcO···HOH) in both IL. At ratios between 2 and 3 ($\chi(H_2O)$ = 0.667–0.750) the water molecules in ILA can be bound to acetate only in the second coordination sphere (AcO···HOH···O(H_2O)). Thus, starting from this moment, the increase of the water fraction should rapidly result in the formation of H-bonds between multiple water molecules, thus creating "free" water. In contrast, in the IL**E**, even if acetate anions are saturated, up to five additional water molecules can be strongly coordinated by the cation via etheric oxygen atoms (HOH···$O_{(etheric)}$). As a result, in the IL**E** water pockets are not expected up to molecular water fractions $\chi(H_2O)$ = 0.82–0.85. Similarly, much higher number of water molecules will be necessary to isolate hydrated ions of IL**E** and make the behavior of the H_2O-IL mixture similar to that of a diluted aqueous solution.

5. Conclusions

This work illustrates in detail the interactions between water and cations of ionic liquid in water miscible ionic liquids within a wide range of water concentrations. Two new water miscible acetate-based ionic liquids with aliphatic substituted and etheric substituted cation ([BMPyr]AcO and [mPEG$_n$MPyr]AcO) were proposed and synthetized. Electrochemical potential window of as prepared electrolytes was established as 2.88 V for [BMPyr]AcO and 2.26 V for [mPEG$_n$MPyr]AcO. Molecular state of water in water – IL mixtures in a wide concentration range was characterized with the help of ATR-FTIR spectroscopy and MD modeling and was correlated with specific conductivity. The results demonstrated that water molecules can strongly interact not only with acetate anions but also with etheric-substituted MPyr cations. Molecular organization of the electrolyte and its conductivity strongly depend on the water content and this dependence differs between ILs with aliphatic and etheric substituted cation. More in details:

1) For molecular ratios between water and ionic liquid n(H_2O) / n(IL) $\leq$ 3 both ATR-FTIR spectra evolution with water dilution and MD simulations indicate strong preferential H-bonding of water molecules to acetate anion. In this concentration range the conductivity of the electrolyte does not vary significantly with water content.

2) For molecular ratios between water and ionic liquid n(H_2O)/n (IL) greater than 3 both infrared spectra and MD simulations suggest different molecular structure evolution for ionic liquids with etheric substituted and aliphatic substituted cation.

In the mixtures with [mPEG$_n$MPyr]AcO, the water molecules stay coordinated by oxygen atoms of etheric groups in the cation which can create H-bonds with up to 5–6 molecules. These H-

bonds are initially less probable than water-acetate H-bonds, however, their relative probability increases with dilution. As a result, water pockets do not form up to $n(H_2O)$ / n(IL**E**) = 7–8. This is coherent with a very insignificant conductivity increase with dilution of [mPEG$_n$MPyr]AcO within this concentration domain.

In contrast, in the mixtures of water with aliphatic substituted [BMPyr]AcO, the probability of H-bonding between water molecules ($HOH\cdots O_{(H2O)}$) increases and the probability of H-bonding between water and acetate (HOH···OAc) decreases with dilution. This is expected to result in the formation of water clusters starting from $n(H_2O)/n(IL) = 3$. This correlates with the experimentally observed conductivity growth with dilution in this concentrations range.

Water clusters form hence at significantly higher water contents in [mPEG$_n$MPyr]AcO than in [BMPyr]AcO because of water-cation interactions.

3) Once "free" water phase with water-water hydrogen bonds is formed, it very rapidly grows in both ILs, which is expected to decrease viscosity and hence increase conductivity. In the formed water clusters, the charge transfer is ensured only by hydrated ions (mainly acetate anions because of their relatively higher mobility if compared to the cation), which should lead to the observed conductivity decrease at high dilutions. Transition from the conductivity increase with water (behavior expected for slightly water diluted IL) to the conductivity decrease with dilution (behavior typical for diluted aqueous solutions with H_2O fraction increase) occurs at molar water to IL ratios $n(H_2O)$ / n(IL) = 33 for aliphatic substituted [BMPyr]AcO and at $n(H_2O)$ / n(IL) = 145 for [mPEG$_n$-MPyr]AcO.

Finally, etheric substitution in IL cation can significantly modify molecular structure of water - IL mixtures and this structure permanence versus dilution.

CRediT authorship contribution statement

D. Kurchavov: Investigation, Methodology, Visualization, Validation, Data curation, Formal analysis, Conceptualization, Writing – original draft, Writing – review & editing. **U. Rustambek:** Investigation, Data curation, Formal analysis, Validation. **M. Haddad:** Investigation, Validation. **A. Ottochian:** Supervision, Data curation, Validation, Writing – review & editing. **G. Lefèvre:** Methodology, Validation, Writing – review & editing. **I. Ciofini:** Methodology, Validation, Writing – review & editing. **V. Lair:** Methodology, Validation, Writing – review & editing. **P. Volovitch:** Conceptualization, Methodology, Validation, Visualization, Supervision, Writing – original draft, Writing – review & editing.

Data availability

Data will be made available on request.

Declaration of Competing Interest

The authors declare that they have no known competing financial interests or personal relationships that could have appeared to influence the work reported in this paper.

Appendix A. Supplementary data

Supplementary data to this article can be found online at https://doi.org/10.1016/j.molliq.2022.120564.

References

[1] A. Taheri, B. Lai, C. Cheng, Y. Gu, Brønsted acid ionic liquid-catalyzed reductive Friedel-Crafts alkylation of indoles and cyclic ketones without using an external reductant, Green Chem. 17 (2015) 812–816, https://doi.org/10.1039/c4gc01299b.
[2] R.P. Swatloski, S.K. Spear, J.D. Holbrey, R.D. Rogers, Dissolution of cellose with ionic liquids, J. Am. Chem. Soc. 124 (2002) 4974–4975, https://doi.org/10.1021/ja025790m.
[3] D. Freudenmann, S. Wolf, M. Wolff, C. Feldmann, Ionic liquids: New perspectives for inorganic synthesis?, Angew Chemie - Int. Ed. 50 (2011) 11050–11060, https://doi.org/10.1002/anie.201100904.
[4] D.R. Macfarlane, N. Tachikawa, M. Forsyth, J.M. Pringle, P.C. Howlett, G.D. Elliott, J.H. Davis, M. Watanabe, P. Simon, C.A. Angell, Energy applications of ionic liquids, Energy Environ. Sci. 7 (2014) 232–250, https://doi.org/10.1039/c3ee42099j.
[5] S. Caporali, F. Ghezzi, A. Giorgetti, A. Lavacchi, A. Tolstogouzov, U. Bardi, Interaction between an imidazolium based ionic liquid and the AZ91D magnesium alloy, Adv. Eng. Mater. 9 (2007) 185–190, https://doi.org/10.1002/adem.200600250.
[6] N. DeVos, C. Maton, C.V. Stevens, Electrochemical Stability of Ionic Liquids: General Influences and Degradation Mechanisms, ChemElectroChem. 1 (2014) 1258–1270, https://doi.org/10.1002/celc.201402086.
[7] M. Hayyan, F.S. Mjalli, M.A. Hashim, I.M. AlNashef, T.X. Mei, Investigating the electrochemical windows of ionic liquids, J. Ind. Eng. Chem. 19 (2013) 106–112, https://doi.org/10.1016/j.jiec.2012.07.011.
[8] Z. Xue, L. Qin, J. Jiang, T. Mu, G. Gao, Thermal, electrochemical and radiolytic stabilities of ionic liquids, Phys. Chem. Chem. Phys. 20 (2018) 8382–8402, https://doi.org/10.1039/c7cp07483b.
[9] E. Knipping, C. Aucher, G. Guirado, L. Aubouy, Room temperature ionic liquids: Versus organic solvents as lithium-oxygen battery electrolytes, New J. Chem. 42 (2018) 4693–4699, https://doi.org/10.1039/c8nj00449h.
[10] S. Ravula, N.E. Larm, M.A. Mottaleb, M.P. Heitz, G.A. Baker, Vapor pressure mapping of ionic liquids and low-volatility fluids using graded isothermal thermogravimetric analysis, ChemEngineering. 3 (2019) 1–12, https://doi.org/10.3390/chemengineering3020042.
[11] D.M. Fox, W.H. Awad, J.W. Gilman, P.H. Maupin, H.C. De Long, P.C. Trulove, Flammability, thermal stability, and phase change characteristics of several trialkylimidazolium salts, Green Chem. 5 (2003) 724–727, https://doi.org/10.1039/b308444b.
[12] C. Comminges, R. Barhdadi, M. Laurent, M. Troupel, Determination of viscosity, ionic conductivity, and diffusion coefficients in some binary systems: Ionic liquids + molecular solvents, J. Chem. Eng. Data. 51 (2006) 680–685, https://doi.org/10.1021/je0504515.
[13] S. Jiang, Y. Hu, Y. Wang, X. Wang, Viscosity of Typical Room-Temperature Ionic Liquids: A Critical Review, J. Phys. Chem. Ref. Data. 48 (2019), https://doi.org/10.1063/1.5090486.
[14] M. Klahn, C. Stüber, A. Seduraman, P. Wu, What determines the miscibility of ionic liquids with water? Identification of the underlying factors to enable a straightforward prediction, J. Phys. Chem. B. 114 (2010) 2856–2868, https://doi.org/10.1021/jp1000557.
[15] L.M. Galán Sánchez, J.R. Espel, F. Onink, G.W. Meindersma, A.B. De Haan, Density, viscosity, and surface tension of synthesis grade imidazolium, pyridinium, and pyrrolidinium based room temperature ionic liquids, J. Chem. Eng. Data. 54 (2009) 2803–2812, https://doi.org/10.1021/je800710p.
[16] K. Tsunashima, M. Sugiya, Physical and electrochemical properties of low-viscosity phosphonium ionic liquids as potential electrolytes, Electrochem. Commun. 9 (2007) 2353–2358, https://doi.org/10.1016/j.elecom.2007.07.003.
[17] A. Jarosik, S.R. Krajewski, A. Lewandowski, P. Radzimski, Conductivity of ionic liquids in mixtures, J. Mol. Liq. 123 (2006) 43–50, https://doi.org/10.1016/j.molliq.2005.06.001.
[18] S. Fendt, S. Padmanabhan, H.W. Blanch, J.M. Prausnitz, Viscosities of acetate or chloride-based ionic liquids and some of their mixtures with water or other common solvents, J. Chem. Eng. Data. 56 (2011) 31–34, https://doi.org/10.1021/je1007235.
[19] A. Stoppa, O. Zech, W. Kunz, R. Buchner, The conductivity of imidazolium-based ionic liquids from (-35 to 195) °c. A. variation of cations alkyl chain, J. Chem. Eng. Data. 55 (2010) 1768–1773, https://doi.org/10.1021/je900789j.
[20] T. Welton, Ionic liquids: a brief history, Biophys. Rev. 10 (2018) 691–706, https://doi.org/10.1007/s12551-018-0419-2.
[21] C. Li, B. Knierim, C. Manisseri, R. Arora, H.V. Scheller, M. Auer, K.P. Vogel, B.A. Simmons, S. Singh, Comparison of dilute acid and ionic liquid pretreatment of switchgrass: Biomass recalcitrance, delignification and enzymatic saccharification, Bioresour. Technol. 101 (2010) 4900–4906, https://doi.org/10.1016/j.biortech.2009.10.066.
[22] M. Armand, F. Endres, D.R. MacFarlane, H. Ohno, B. Scrosati, Ionic-liquid materials for the electrochemical challenges of the future, Nat. Mater. 8 (2009) 621–629, https://doi.org/10.1038/nmat2448.
[23] Z. Wang, L. Fu, H. Xu, Y. Shang, L. Zhang, J. Zhang, Density, viscosity, and conductivity for the binary systems of water + dual amino-functionalized ionic liquids, J. Chem. Eng. Data. 57 (2012) 1057–1063, https://doi.org/10.1021/je2007549.
[24] K.R. Seddon, A. Stark, M.-J.-J. Torres, Influence of chloride, water, and organic solvents on the physical properties of ionic liquids, Pure Appl. Chem. 72 (2000) 2275–2287, https://doi.org/10.1351/pac200072122275.
[25] T.A. Fadeeva, P. Husson, J.A. Devine, M.F. Costa Gomes, S.G. Greenbaum, E.W. Castner, Interactions between water and 1-butyl-1-methylpyrrolidinium ionic liquids, J. Chem. Phys. 143 (2015) 1–13, https://doi.org/10.1063/1.4928065.
[26] Y. Zhang, R. Ye, D. Henkensmeier, R. Hempelmann, R. Chen, "Water-in-ionic liquid" solutions towards wide electrochemical stability windows for aqueous

rechargeable batteries, Electrochim. Acta. 263 (2018) 47–52, https://doi.org/10.1016/j.electacta.2018.01.050.
[27] R. Chen, R. Hempelmann, Ionic liquid-mediated aqueous redox flow batteries for high voltage applications, Electrochem. Commun. 70 (2016) 56–59, https://doi.org/10.1016/j.elecom.2016.07.003.
[28] S. Chen, R. Lan, J. Humphreys, S. Tao, Effect of cation size on alkali acetate-based 'water-in-bisalt' electrolyte and its application in aqueous rechargeable lithium battery, Appl. Mater. Today. 20 (2020), https://doi.org/10.1016/j.apmt.2020.100728.
[29] J.G. Huddleston, A.E. Visser, W.M. Reichert, H.D. Willauer, G.A. Broker, R.D. Rogers, Characterization and comparison of hydrophilic and hydrophobic room temperature ionic liquids incorporating the imidazolium cation, Green Chem. 3 (2001) 156–164, https://doi.org/10.1039/b103275p.
[30] S. Feng, G.A. Voth, Molecular dynamics simulations of imidazolium-based ionic liquid/water mixtures: Alkyl side chain length and anion effects, Fluid Phase Equilib. 294 (2010) 148–156, https://doi.org/10.1016/j.fluid.2010.02.034.
[31] H.E. Bailey, Y.L. Wang, M.D. Fayer, The influence of hydrophilicity on the orientational dynamics and structures of imidazolium-based ionic liquid/water binary mixtures, J. Chem. Phys. 149 (2018), https://doi.org/10.1063/1.5038563.
[32] W. Jiang, Y. Wang, G.A. Voth, Molecular dynamics simulation of nanostructural organization in ionic liquid/water mixtures, J. Phys. Chem. B. 111 (2007) 4812–4818, https://doi.org/10.1021/jp0671421.
[33] J.N. Canongia Lopes, M.F. Costa Gomes, A.A.H. Pádua, Nonpolar, polar, and associating solutes in ionic liquids, J. Phys. Chem. B. 110 (2006) 16816–16818, https://doi.org/10.1021/jp063603r.
[34] A.R. Porter, S.Y. Liem, P.L.A. Popelier, Room temperature ionic liquids containing low water concentrations-a molecular dynamics study, Phys. Chem. Chem. Phys. 10 (2008) 4240–4248, https://doi.org/10.1039/b718011j.
[35] S.H.Y. Wang, H. Li, A theoretical investigation of the interactions between water molecules and ionic liquids, J. Phys. Chem. B. 110 (2006) 24646–24651, https://doi.org/10.1021/jp064134w.
[36] T. Méndez-Morales, J. Carrete, Ó. Cabeza, L.J. Gallego, L.M. Varela, Molecular dynamics simulation of the structure and dynamics of water-1-alkyl-3-methylimidazolium ionic liquid mixtures, J. Phys. Chem. B. 115 (2011) 6995–7008, https://doi.org/10.1021/jp202692g.
[37] T. Koishi, Molecular Dynamics Study of the Effect of Water on Hydrophilic and Hydrophobic Ionic Liquids, J. Phys. Chem. B. 122 (2018) 12342–12350, https://doi.org/10.1021/acs.jpcb.8b07774.
[38] A. Dominguez-Vidal, N. Kaun, M.J. Ayora-Cañada, B. Lendl, Probing intermolecular interactions in water/ionic liquid mixtures by far-infrared spectroscopy, J. Phys. Chem. B. 111 (2007) 4446–4452, https://doi.org/10.1021/jp068777n.
[39] L. Cammarata, S.G. Kazarian, P.A. Salter, T. Welton, Molecular states of water in room temperature ionic liquids, Phys. Chem. Chem. Phys. 3 (2001) 5192–5200, https://doi.org/10.1039/b106900d.
[40] H. Abe, T. Takekiyo, M. Shigemi, Y. Yoshimura, S. Tsuge, T. Hanasaki, K. Ohishi, S. Takata, J.I. Suzuki, Direct evidence of confined water in room-temperature ionic liquids by complementary use of small-angle X-ray and neutron scattering, J. Phys. Chem. Lett. 5 (2014) 1175–1180, https://doi.org/10.1021/jz500299z.
[41] M. Brehm, H. Weber, A.S. Pensado, A. Stark, B. Kirchner, Liquid structure and cluster formation in ionic liquid/water mixtures - An extensive ab initio molecular dynamics study on 1-ethyl-3-methylimidazolium acetate/water mixtures - Part 2, Zeitschrift Fur Phys, Chemie. 227 (2013) 177–203, https://doi.org/10.1524/zpch.2012.0327.
[42] V.H. Paschoal, L.F.O. Faria, M.C.C. Ribeiro, Vibrational Spectroscopy of Ionic Liquids, Chem. Rev. 117 (2017) 7053–7112, https://doi.org/10.1021/acs.chemrev.6b00461.
[43] M.I. Barba, M.S. Larrechi, A. Coronas, Quantitative analysis of free water in ionic liquid-water mixtures, Talanta. 199 (2019) 407–414, https://doi.org/10.1016/j.talanta.2019.02.087.
[44] T. Köddermann, C. Wertz, A. Heintz, R. Ludwig, The association of water in ionic liquids: A reliable measure of polarity, Angew. Chemie - Int. Ed. 45 (2006) 3697–3702, https://doi.org/10.1002/anie.200504471.
[45] M. López-Pastor, M.J. Ayora-Cañada, M. Valcárcel, B. Lendl, Association of methanol and water in ionic liquids elucidated by infrared spectroscopy using two-dimensional correlation and multivariate curve resolution, J. Phys. Chem. B. 110 (2006) 10896–10902, https://doi.org/10.1021/jp057398b.
[46] O. Palumbo, F. Trequattrini, J.B. Brubach, P. Roy, A. Paolone, Molecular assembling in mixtures of hydrophilic 1-butyl-1-methylpyrrolidinium dicyanamide ionic liquid and water, Appl. Sci. 10 (2020), https://doi.org/10.3390/app10144837.
[47] S. Dasari, B.S. Mallik, Association of Nucleobases in Hydrated Ionic Liquid from Biased Molecular Dynamics Simulations, J. Phys. Chem. B. 122 (2018) 9635–9645, https://doi.org/10.1021/acs.jpcb.8b05778.
[48] S. Dasari, B.S. Mallik, Biosolvation Nature of Ionic Liquids: Molecular Dynamics Simulation of Methylated Nucleobases in Hydrated 1-Ethyl-3-methylimidazolium Acetate, ACS Omega. 3 (2018) 8344–8354, https://doi.org/10.1021/acsomega.8b01231.
[49] E.E. Fenn, D.E. Moilanen, N.E. Levinger, M.D. Fayer, Water dynamics and interactions in water-polyether binary mixtures, J. Am. Chem. Soc. 131 (2009) 5530–5539, https://doi.org/10.1021/ja809261d.
[50] K. Kim, H.J. Jang, C.Y. Shin, Safety evaluation of polyethylene glycol (PEG) compounds for cosmetic use, Toxicol. Res. 31 (2015) 105–136, https://doi.org/10.5487/TR.2015.31.2.105.
[51] D. Hutanu, Recent Applications of Polyethylene Glycols (PEGs) and PEG Derivatives, Mod. Chem. Appl. 02 (2014) 2–7, https://doi.org/10.4172/2329-6798.1000132.
[52] K. Shameli, M. Bin Ahmad, S.D. Jazayeri, S. Sedaghat, P. Shabanzadeh, H. Jahangirian, M. Mahdavi, Y. Abdollahi, Synthesis and characterization of polyethylene glycol mediated silver nanoparticles by the green method, Int. J. Mol. Sci. 13 (2012) 6639–6650, https://doi.org/10.3390/ijms13066639.
[53] K. Yoshii, T. Uto, T. Onishi, D. Kosuga, N. Tachikawa, Y. Katayama, Ether-Functionalized Pyrrolidinium-Based Room Temperature Ionic Liquids: Physicochemical Properties, Molecular Dynamics, and the Lithium Ion Coordination Environment, ChemPhysChem. 22 (2021) 1584–1594, https://doi.org/10.1002/cphc.202100380.
[54] D. Brouillette, D.E. Irish, N.J. Taylor, G. Perron, M. Odziemkowski, J.E. Desnoyers, Stable solvates in solution of lithium bis(trifluoromethylsulfone) imide in glymes and other aprotic solvents: Phase diagrams, crystallography and Raman spectroscopy, Phys. Chem. Chem. Phys. 4 (2002) 6063–6071, https://doi.org/10.1039/b203776a.
[55] T. Watkins, A. Kumar, D.A. Buttry, Supporting Information Designer Ionic Liquids for Reversible Electrochemical Deposition / Dissolution of Mg, J. Am. Chem. Soc. 138 (2016) 1–9, https://doi.org/10.1021/jacs.5b11031.
[56] M. Kar, O. Tutusaus, D.R. MacFarlane, R. Mohtadi, Novel and versatile room temperature ionic liquids for energy storage, Energy Environ. Sci. 12 (2019) 566–571, https://doi.org/10.1039/c8ee02437e.
[57] X. Gao, A. Mariani, S. Jeong, X. Liu, X. Dou, M. Ding, A. Moretti, S. Passerini, Prototype rechargeable magnesium batteries using ionic liquid electrolytes, J. Power Sources. 423 (2019) 52–59, https://doi.org/10.1016/j.jpowsour.2019.03.049.
[58] L. Garcia-Quintana, F. Chen, N. Ortiz-Vitoriano, Y. Zhang, L.A. O'Dell, D.R. MacFarlane, M. Forsyth, A.M. Bond, P.C. Howlett, C. Pozo-Gonzalo, Unravelling the Role of Speciation in Glyme: Ionic Liquid Hybrid Electrolytes for Na−O 2 Batteries, Batter. Supercaps. 4 (2021) 513–521, https://doi.org/10.1002/batt.202000261.
[59] L.V.N.R. Ganapatibhotla, J. Zheng, D. Roy, S. Krishnan, PEGylated imidazolium ionic liquid electrolytes: Thermophysical and electrochemical properties, Chem. Mater. 22 (2010) 6347–6360, https://doi.org/10.1021/cm102263s.
[60] D. Kasprzak, I. Stępniak, M. Galiński, Acetate- and lactate-based ionic liquids: Synthesis, characterisation and electrochemical properties, J. Mol. Liq. 264 (2018) 233–241, https://doi.org/10.1016/j.molliq.2018.05.059.
[61] N. Frenzel, J. Hartley, G. Frisch, Voltammetric and spectroscopic study of ferrocene and hexacyanoferrate and the suitability of their redox couples as internal standards in ionic liquids, Phys. Chem. Chem. Phys. 19 (2017) 28841–28852, https://doi.org/10.1039/c7cp05483a.
[62] R. Dennington, T.A. Keith, J.M. Millam, GaussView, Version 6, Semichem Inc., Shawnee Mission. KS. (2016).
[63] M.J. Frisch, G.W. Trucks, H.B. Schlegel, G.E. Scuseria, M.A. Robb, J.R. Cheeseman, G. Scalmani, V. Barone, G.A. Petersson, X. Nakatsuji, H.; Li, M. Caricato, A. V. Marenich, J. Bloino, B.G. Janesko, R. Gomperts, B. Mennucci, D.J. Hratch, Gaussian 16, Revision C.01, Gaussian, Inc., Wallingford CT. (2016).
[64] J. Wang, W. Wang, P.A. Kollman, D.A. Case, Automatic atom type and bond type perception in molecular mechanical calculations, J. Mol. Graph. Model. 25 (2006) 247–260.
[65] K. Yoshii, T. Uto, N. Tachikawa, Y. Katayama, The effects of the position of the ether oxygen atom in pyrrolidinium-based room temperature ionic liquids on their physicochemical properties, Phys. Chem. Chem. Phys. 22 (2020) 19480–19491, https://doi.org/10.1039/d0cp02662j.
[66] C.J. Cramer, Essentials of Computational Chemistry: Theories and Models, 2nd ed., John Wiley & Sons, 2013, 2013.
[67] L. Martínez, R. Andrade, E.G. Birgin, J.M. Martínez, Packmol: A package for building initial configurations for molecular dynamics simulations, J. Comput. Chem. 30 (2009) 2157–2164.
[68] S. Plimpton, Fast Parallel Algorithms for Short-Range Molecular Dynamics, J. Comput. Phys. 117 (2008) 1–19.
[69] LAMMPS web site, (n.d.).
[70] R. Ludwig, Water: From clusters to the bulk, Angew. Chemie - Int. Ed. 40 (2001) 1808–1827, https://doi.org/10.1002/1521-3773(20010518)40:10<1808::AID-ANIE1808>3.0.CO;2-1.
[71] Z. Bin Zhou, H. Matsumoto, K. Tatsumi, Cyclic quaternary ammonium ionic liquids with perfluoroalkyltrifluoroborates: Synthesis, characterization, and properties, Chem. - A Eur. J. 12 (2006) 2196–2212, https://doi.org/10.1002/chem.200500930.
[72] S. Fang, Z. Zhang, Y. Jin, L. Yang, S.I. Hirano, K. Tachibana, S. Katayama, New functionalized ionic liquids based on pyrrolidinium and piperidinium cations with two ether groups as electrolytes for lithium battery, J. Power Sources. 196 (2011) 5637–5644, https://doi.org/10.1016/j.jpowsour.2011.02.047.
[73] S. Pandian, K.S. Hariharan, S.P. Adiga, S.M. Kolake, Evaluation of Electrochemical Stability and Li-ion Interactions in Ether Functionalized Pyrrolidinium and Phospholanium Ionic Liquids, J. Electrochem. Soc. 167 (2020), https://doi.org/10.1149/1945-7111/ab8061.
[74] M. Moreno, M. Montanino, M. Carewska, G.B. Appetecchi, S. Jeremias, S. Passerini, Water-soluble, triflate-based, pyrrolidinium ionic liquids, Electrochim. Acta. 99 (2013) 108–116, https://doi.org/10.1016/j.electacta.2013.03.046.

[75] J. Bowers, C.P. Butts, P.J. Martin, M.C. Vergara-Gutierrez, R.K. Heenan, Aggregation Behavior of Aqueous Solutions of Ionic Liquids, Langmuir. 20 (2004) 2191–2198, https://doi.org/10.1021/la035940m.
[76] W.A. Henderson, N.R. Brooks, W.W. Brennessel, V.G. Young, Triglyme-Li+ Cation Solvate Structures: Models for Amorphous Concentrated Liquid and Polymer Electrolytes (I), Chem. Mater. 15 (2003) 4679–4684, https://doi.org/10.1021/cm034351z.
[77] W. Silva, M. Zanatta, A.S. Ferreira, M.C. Corvo, E.J. Cabrita, Revisiting ionic liquid structure-property relationship: A critical analysis, Int. J. Mol. Sci. 21 (2020) 1–37, https://doi.org/10.3390/ijms21207745.
[78] N. Yaghini, L. Nordstierna, A. Martinelli, Effect of water on the transport properties of protic and aprotic imidazolium ionic liquids-an analysis of self-diffusivity, conductivity, and proton exchange mechanism, Phys. Chem. Chem. Phys. 16 (2014) 9266–9275, https://doi.org/10.1039/c4cp00527a.
[79] M.I. Cabaço, M. Besnard, Y. Danten, J.A.P. Coutinho, Carbon dioxide in 1-butyl-3-methylimidazolium acetate. I. Unusual solubility investigated by Raman spectroscopy and DFT calculations, J. Phys. Chem. A. 116 (2012) 1605–1620, https://doi.org/10.1021/jp211211n.
[80] B. Bednarska-Bolek, R. Jakubas, G. Bator, J. Baran, Vibrational study of the structural phase transition in bis(pyrrolidinium)-chloride-hexachloroantimonate(V) by infrared spectroscopy, J. Mol. Struct. 614 (2002) 151–157, https://doi.org/10.1016/S0022-2860(02)00235-1.
[81] Y. Chen, Y. Cao, Y. Zhang, T. Mu, Hydrogen bonding between acetate-based ionic liquids and water: Three types of IR absorption peaks and NMR chemical shifts change upon dilution, J. Mol. Struct. 1058 (2014) 244–251, https://doi.org/10.1016/j.molstruc.2013.11.010.
[82] M. Thomas, M. Brehm, O. Hollóczki, Z. Kelemen, L. Nyulászi, T. Pasinszki, B. Kirchner, Simulating the vibrational spectra of ionic liquid systems: 1-Ethyl-3-methylimidazolium acetate and its mixtures, J. Chem. Phys. 141 (2014), https://doi.org/10.1063/1.4887082.
[83] C. Laurence, S. Mansour, D. Vuluga, J. Legros, Measurement of the hydrogen bond acceptance of ionic liquids and green solvents by the19F solvatomagnetic comparison method, Green Chem. 23 (2021) 1816–1822, https://doi.org/10.1039/d0gc04104a.
[84] K. Matsuura, H., Fukuhara,, Conformational analysis of poly(oxyethylene) chain in aqueous solution as a hydrophilic moiety of nonionic surfactants, J. Mol. Struct. 126 (1985) 251–260. (https://doi.org/10.1016/0022-2860(85)80118-6, https://doi.org/10.1016/0022-2860(85)80118-6.
[85] S. Dasari, B.S. Mallik, Conformational dynamics of polymers in ethylammonium nitrate from advanced sampling methods, Comput. Mater. Sci. 203 (2022), https://doi.org/10.1016/j.commatsci.2021.111072.
[86] K. Ito, H.J. Bernstein, the Vibrational Spectra of the Formate, Acetate, and Oxalate Ions, Can. J. Chem. 34 (1956) 170–178, https://doi.org/10.1139/v56-021.
[87] N. Yaghini, J. Pitawala, A. Matic, A. Martinelli, Effect of water on the local structure and phase behavior of imidazolium-based protic ionic liquids, J. Phys. Chem. B. 119 (2015) 1611–1622, https://doi.org/10.1021/jp510691e.
[88] P. Bharmoria, H. Gupta, V.P. Mohandas, P.K. Ghosh, A. Kumar, Temperature invariance of NaCl solubility in water: Inferences from salt-water cluster behavior of NaCl, KCl, and NH4Cl, J. Phys. Chem. B. 116 (2012) 11712–11719, https://doi.org/10.1021/jp307261g.
[89] L. Cammarata, S.G. Kazarian, P.A. Salter, T. Welton, Molecular states of water in room temperature ionic liquidsElectronic Supplementary Information available. See http://www.rsc.org/suppdata/cp/b1/b106900d/, Phys. Chem. Chem. Phys. 3 (2001) 5192–5200, https://doi.org/10.1039/b106900d.
[90] P. Laurson, P. Raudsepp, H. Kaldmäe, A. Kikas, U. Mäeorg, The deconvolution of FTIR-ATR spectra to five Gaussians for detection of small changes in plant-water clusters, AIP Adv. 10 (2020), https://doi.org/10.1063/5.0011700.
[91] K.B. Møller, R. Rey, J.T. Hynes, Hydrogen bond dynamics in water and ultrafast infrared spectroscopy: A theoretical study, J. Phys. Chem. A. 108 (2004) 1275–1289, https://doi.org/10.1021/jp035935r.
[92] G. Li, Y.Y. Zhang, Q. Li, C. Wang, Y. Yu, B. Zhang, H.S. Hu, W. Zhang, D. Dai, G. Wu, D.H. Zhang, J. Li, X. Yang, L. Jiang, Infrared spectroscopic study of hydrogen bonding topologies in the smallest ice cube, Nat. Commun. 11 (2020) 2–7, https://doi.org/10.1038/s41467-020-19226-6.
[93] C. Boissière, J.B. Brubach, A. Mermet, G. Marzi De, C. Bourgaux, E. Prouzet, P. Roy, Water confined in lamellar structures of AOT surfactants: An infrared investigation, J. Phys. Chem. B. 106 (2002) 1032–1035, https://doi.org/10.1021/jp012724i.
[94] S. Biswas, B.S. Mallik, Vibration Spectral Dynamics of Weakly Coordinating Water Molecules near an Anion: FPMD Simulations of an Aqueous Solution of Tetrafluoroborate, J. Phys. Chem. B. 123 (2019) 2135–2146, https://doi.org/10.1021/acs.jpcb.9b00069.